RÉPUBLIQUE ALGÉRIENNE DÉMOCRATIQUE ET POPULAIRE
MINISTÈRE DE L'ENSEIGNEMENT SUPÉRIEUR ET DE LA RECHERCHE SCIENTIFIQUE

ÉCOLE NATIONALE POLYTECHNIQUE

المدرسة الوطنية المتعددة التقنيات
Ecole Nationale Polytechnique

Département d'Électronique

Final Year Project Dissertation

In partial fulfillment of the requirements for the State Engineer's Degree in Electronics Engineering

---

Study and Simulation of Quantum Illumination and Its Impact on Detection

---

MEDDAH Ahmed Assem

Presented and publicly defended on (21/06/2026)

Jury composition:

Chairman:	Pr. TOUHAMI Rachida	Ecole Nationale Polytechnique
Examiner:	Dr. MOKRAOUI Amine	Ecole Nationale Polytechnique
Supervisor:	Dr. NOUAR Nabila	Ecole Nationale Polytechnique

ENP 2026

RÉPUBLIQUE ALGÉRIENNE DÉMOCRATIQUE ET POPULAIRE
MINISTÈRE DE L'ENSEIGNEMENT SUPÉRIEUR ET DE LA RECHERCHE SCIENTIFIQUE

ÉCOLE NATIONALE POLYTECHNIQUE

المدرسة الوطنية المتعددة التقنيات
Ecole Nationale Polytechnique

Département d'Électronique

Final Year Project Dissertation

In partial fulfillment of the requirements for the State Engineer's Degree in Electronics Engineering

---

Study and Simulation of Quantum Illumination and Its Impact on Detection

---

MEDDAH Ahmed Assem

Presented and publicly defended on (21/06/2026)

Jury composition:

Chairman:	Pr. TOUHAMI Rachida	Ecole Nationale Polytechnique
Examiner:	Dr. MOKRAOUI Amine	Ecole Nationale Polytechnique
Supervisor:	Dr. NOUAR Nabila	Ecole Nationale Polytechnique

ENP 2026

RÉPUBLIQUE ALGÉRIENNE DÉMOCRATIQUE ET POPULAIRE
MINISTÈRE DE L'ENSEIGNEMENT SUPÉRIEUR ET DE LA RECHERCHE SCIENTIFIQUE

ÉCOLE NATIONALE POLYTECHNIQUE

المدرسة الوطنية المتعددة التقنيات
Ecole Nationale Polytechnique

Département d'Électronique

Mémoire de Projet de Fin d'Études

Pour l'obtention du diplôme d'Ingénieur d'État en Électronique

---

Étude et Simulation de l'Illumination Quantique et Son Impact sur la Détection

---

MEDDAH Ahmed Assem

Présenté et soutenu publiquement le (21/06/2026)

Composition du Jury :

Présidente :	Pr. TOUHAMI Rachida	École Nationale Polytechnique
Examinateur :	Dr. MOKRAOUI Amine	École Nationale Polytechnique
Promotrice :	Dr. NOUAR Nabila	École Nationale Polytechnique

ENP 2026

ملخص

الإيضاء الكمي بروتوكول استشعار يعِد بتحقيق ميزة في الكشف مقارنةً بالرادار الكلاسيكي في البيئات المشوشة وضعيفة الإشارة، وذلك باستغلال الأزواج الكمية المتشابكة من الإشارة والمرجع. وعلى الرغم من الضمانات النظرية الراسخة لا سيما تحسّن مقداره ٦ ديسيبل في أُس خطأ الكشف مقارنةً بالرادار الكلاسيكي ذي الحالة المتماسكة تظل الآثار العملية لهذه الميزة في سياق هندسة الرادار إلى حدٍّ بعيد غير مستكشَفة.

تُقيِّم هذه الأطروحة ادعاءات الإيضاء الكمي من منظور هندسة الإلكترونيات، بهدفَين مزدوجين: التحقق من الفيزياء النظرية، وترجمتها إلى مقاديرِ هندسية قابلة للتطبيق في مجال الرادار. تُنفذ ثلاثة مناهج محاكاة متصاعدة الدقة وتُقارن: نموذج توضيحي موجه نحو الرادار، ومحاكاة في فضاء فوك دقيقة فيزيائياً، ومحاكاة فعّالة قائمة على مصفوفة التباين الغاوسية. وتتفق المناهج الثلاثة على أن مستقبِل الارتباط القابل للتطبيق يمنح ميزةً تبلغ نحو ٣ ديسيبل مقارنةً بالاستراتيجية الكلاسيكية ذات الطاقة المكافئة، وهو ما يتسق مع السقف النظري البالغ ٦ ديسيبل المُحدد للمستقبِل المشترك الأمثل.

يُطوِّر بعد ذلك إطار ترجمة شفاف يربط معاملات الرادار الكلاسيكية --- المدى، والمساحة الرادارية المكافئة، وقدرة الإرسال، وحرارة النظام --- بمقادير الفيزياء الكمية المتمثلة في الانتقالية η والخلفية الحرارية N_B، عبر معادلة الرادار وعامل بوز. يكشف تطبيق هذا الجسر على سيناريوهاتِ الميكروويف الواقعية أنه عند ترددات النطاق ط ومدى بمقياس الكيلومتر، ينهار كلا الكاشفين إلى أداء عشوائي بسبب خسائر انتشار كارثية وخلفيات حرارية هائلة. غير أن نسبة الميزة الكمية مقارنةً بالكلاسيكية تظل محفوظةً عند نحو ٨،٢ ديسيبل، مما يؤكد أن الميزة الكمية تُمثِّل تحسُّناً حقيقياً في كفاءة الكشف لا وسيلةً لرصد أهداف لا يمكن كشفها بطريقة أخرى --- وهو نتيجة تُفسِّر كمياً السبب في عدم نشر رادار الإيضاء الكمي حتى الآن.

الكلمات المفتاحية: الإيضاء الكمي --- الرادار الكمي --- الرادار الكلاسيكي --- نظرية الكشف --- الحالات الغاوسية --- مصفوفة التباين --- حد شيرنوف الكمي --- نسبة الإشارة إلى الضجيج --- المساحة الرادارية المكافئة --- الميزة الكمية

Résumé

L'illumination quantique (IQ) est un protocole de télédétection qui promet un avantage sur le radar classique dans des environnements bruités et à faible signal, en exploitant des paires signal-idler quantiquement intriquées. Malgré des garanties théoriques bien établies, notamment une amélioration de 6 dB de l'exposant d'erreur par rapport au radar classique à état cohérent,les implications pratiques de cet avantage en termes d'ingénierie radar restent largement inexplorées. Cette thèse évalue les affirmations de l'illumination quantique dans une perspective d'ingénierie électronique, avec le double objectif de valider la physique théorique et de la traduire en grandeurs propres à l'ingénierie radar. Trois approches de simulation de rigueur croissante sont mises en œuvre et comparées : une démonstration illustrative orientée radar, une simulation dans l'espace de Fock physiquement rigoureuse, et une simulation efficace basée sur la matrice de covariance gaussienne. Les trois approches s'accordent : le récepteur de corrélation implémentable apporte environ 3 dB d'avantage sur une stratégie classique à énergie équivalente, ce qui est cohérent avec le plafond théorique de 6 dB établi pour le récepteur joint optimal. Un cadre de traduction transparent est ensuite développé, faisant correspondre les paramètres radar classiques : portée, section efficace radar, puissance d'émission et température du système aux grandeurs de la physique quantique que sont la transmissivité η et le fond thermique N_B, via l'équation radar et le facteur de Bose. L'application de ce pont à des scénarios micro-ondes réalistes révèle qu'en bande X et pour des portées kilométriques, les deux détecteurs s'effondrent à une performance aléatoire en raison de pertes de propagation catastrophiques et de fonds thermiques considérables. Pourtant, le ratio d'avantage quantique sur classique reste préservé à environ 2,8 dB, confirmant que l'avantage quantique constitue une amélioration réelle de l'efficacité de détection plutôt qu'un moyen de détecter des cibles autrement indétectables, un résultat qui explique quantitativement pourquoi le radar à illumination quantique n'a pas encore été déployé.

Mots clés : Illumination Quantique , Radar Quantique , Radar Classique, Théorie de la Détection, États Gaussiens , Matrice de Covariance, Borne de Chernoff Quantique, Rapport Signal sur Bruit, Section Efficace Radar, Avantage Quantique.

Abstract

Quantum illumination (QI) is a sensing protocol that promises a detection advantage over classical radar in noisy, low-signal environments by exploiting quantum-entangled signal-idler pairs. Despite well-established theoretical guarantees, notably a 6 dB improvement in the error exponent over coherent-state classical radar, the practical implications of this advantage in radar engineering terms remain largely unexplored. This thesis evaluates the quantum illumination claim from an electronics engineering perspective, with the dual objective of validating the theoretical physics and translating it into radar-engineering quantities. Three simulation approaches of increasing rigour are implemented and compared: an illustrative radar-oriented demonstration, a physically rigorous Fock-space simulation, and an efficient Gaussian-covariance simulation. All three approaches agree: the implementable correlation receiver delivers approximately 3 dB over an energy-matched classical strategy, consistent with the 6 dB theoretical ceiling established for the optimal joint receiver. A transparent translation framework is then developed, mapping classical radar parameters like range, radar cross-section, transmit power, and system temperature to the quantum physics quantities transmissivity eta and thermal background N_B, via the radar equation and the Bose factor. Applying this bridge to realistic microwave scenarios reveals that at X-band frequencies and kilometre-scale ranges, both detectors collapse to chance performance due to catastrophic propagation losses and enormous thermal backgrounds. Yet the quantum-to-classical advantage ratio remains preserved at approximately 2.8 dB throughout, confirming that the quantum advantage is a genuine improvement in detection efficiency rather than a means to detect otherwise undetectable targets, a finding that quantitatively explains why quantum illumination radar has not yet been deployed.

Keywords : Quantum Illumination , Quantum Radar , Classical Radar , Detection Theory, Gaussian States , Covariance Matrix , Quantum Chernoff Bound , Signal-to-Noise Ratio , Radar Cross-Section , Quantum Advantage

Acknowledgments

In the name of Allah, the Most Gracious, the Most Merciful.

All praise is due to Him, for the strength, patience, and guidance that carried this work from its first uncertain beginnings, through its quiet breakthroughs, to its completion.

I would like to express my sincere gratitude to my supervisor, Dr. Nouar, for her trust, her guidance, and the freedom she gave me throughout this work.

I am also grateful to the members of the jury, Dr. Mokraoui and Pr. Touhami, for the time they devoted to reviewing this thesis. My thanks also extend to all the professors of the Department of Electronics Engineering.

My gratitude reaches further back, to my teachers in middle school and high school, who first believed in me and have continued to do so since.

I wish to thank my parents and my entire family. Each of you supported me in your own way, with a patience and care that extended far beyond this work and throughout my life. I am deeply grateful.

Finally, to Vniverse, my second family; to Houssem, Basset, Ibtihal, Maria, and Khaled; your presence has shaped not only my graduation, but everything beyond it. Thank you.

Ascem Meddah ;

Dedication

"We have to live a life of no regrets."

This, to the people who made it possible and worth it.

To my classmates, for the three years we shared and everything we went through together, and to my lab and internship partners; thank you.

To the IEEE committees of 2024 and 2025, and to all their members; especially Jiyuu-da, thank you for still helping even now.

To the VIC: to the older members, for welcoming us and believing in us, and to the younger members, for appreciating us. Thank you.

To all my family, and especially my dear cousins; thank you for all the lifelong support.

To Vniverse, my second family; to Nazim, Ahlam, Mourad, Hiba, Aya, Karim, Mehdi, Miko, Shinso, Moh, Besmala and all the younger ones; to Malik, Djouzi, Imed, Melissa, Said, Amine, Mahmoud, Hafsa, Raouf, Hakim, Amina, Sassi, Ghiles, Issam and all the older ones who still take care of us; I thank you all for the time, effort, love, and care you have given. I will keep loving you all, always.

To my promo and to V Study; to Haithem and Madina, Roudji, Lydia, Amina, and to Louay, Rayan and Ammali; thank you all for trusting the process.

Tarek, Said, Nardjes, Hadjer and Ilham; I saw faith and genuine support in your eyes. Thank you for everything.

To my parents; you didn't just believe in me, you continued to see in me what I couldn't see in myself. No matter how much I complained, you always carried me. This thesis is as much yours as it is mine.

My brother, Mido; when you're old enough to read this, you'll no longer hear "Maybe next time" whenever you want to play chess.

My brother, Adnane, the prodigy, and the one who believes in me in an unbelievable way; thank you for being a fuel to my confidence, and my only ever rival.

To all the versions of myself, past or future, this was nothing but an unwanted path filled with beautiful memories, a wonderful tale, and a chance for the arrow to go farther.

Finally, Houssem, Basset, Ibtihal, Maria, Khaled... Thank you.
Words won't be enough, so I'll use my favorite scene:

"Thank you for loving me."

;

Kiyo V

Table of contents

List of Tables

List of Figures

List of acronyms

General Introduction **15**
Project Context . . . 15
Structure of the manuscript . . . 15

1 Introduction and State of the Art **17**
1.1 Definition . . . 18
1.2 Problem Statement . . . 18
1.3 State of Art . . . 19
1.3.1 A Brief History of Radar . . . 19
1.3.2 A Brief History of Quantum Mechanics . . . 20
1.3.3 From Quantum Sensing to Quantum Illumination . . . 20
1.3.4 Quantum Radar: Principles and Classes . . . 21
1.3.5 Applications of Quantum Radar . . . 23
1.4 Motivation and research Objectives . . . 24
1.4.1 Motivation . . . 24
1.4.2 Research objectives . . . 24
1.5 Contribution . . . 25

2 Classical Radar Fundamentals **26**
2.1 Introduction . . . 28
2.2 What Radar Measures . . . 28
2.3 The Radar Equation Derivation . . . 30
2.4 Noise and the Minimum Detectable Signal . . . 31
2.5 Maximum Range Equation . . . 32
2.6 Monostatic vs Bistatic Radar . . . 33
2.7 Radar Losses . . . 33
2.8 Locating a Target . . . 34
2.9 Radar Cross Section (RCS) . . . 35
2.10 Radar Frequency Bands . . . 36
2.11 Simulations . . . 37
2.11.1 Summary of Key Radar Parameters . . . 41
2.12 Conclusion . . . 41

3 Detection Theory **42**
3.1 Introduction . . . 44

3.2 What "Detection" Means Mathematically . . . 44
3.2.1 Binary Hypothesis Testing Framework . . . 44
3.2.2 Terminology . . . 45
3.2.3 Detection Performance Metrics . . . 45
3.3 Statistical Model for AWGN . . . 47
3.3.1 White Noise Definition . . . 47
3.3.2 Probability Density Functions Under H_0 and H_1 . . . 47
3.3.3 Connection to Detection . . . 49
3.4 The Neyman-Pearson Criterion . . . 49
3.5 Likelihood Ratio Test and Matched Filter . . . 50
3.6 The Deflection Coefficient: A General Detection Metric . . . 50
3.6.1 Definition . . . 50
3.6.2 The deflection coefficient governs the ROC . . . 51
3.6.3 Classical and quantum evaluations . . . 51
3.6.4 Multimode scaling . . . 51
3.7 Receiver Operating Characteristic (ROC) Curves . . . 52
3.7.1 Interpreting ROC Curves . . . 52
3.8 Conclusion . . . 53

4 Discovering Quantum Radars 55
4.1 Introduction: Why Quantum Radar? . . . 57
4.2 The Quantum Illumination Protocol . . . 57
4.2.1 Conceptual Step-by-Step of the QI Protocol . . . 58
4.2.2 Conceptual Diagram of the QI Protocol . . . 59
4.2.3 Key Parameters Defined . . . 59
4.2.4 The Counterintuitive Nature of QI . . . 59
4.3 Core Mathematical Framework . . . 60
4.3.1 Quantum States and Hilbert Spaces . . . 60
4.3.2 Unitary Evolution and Hamiltonians . . . 60
4.3.3 Composite Systems and Tensor Products . . . 60
4.4 What Does a Quantum State Actually Describe? . . . 61
4.4.1 What Phase Means Here: A Relational and Intuitive View . . . 61
4.5 Superposition, Joint Quantum States, and Density Matrices . . . 62
4.5.1 Superposition in Single Systems . . . 62
4.5.2 Density Matrix Formalism . . . 63
4.5.3 Interference, Coherence, and Off-Diagonal Terms . . . 63
4.5.4 Separability and Entanglement . . . 63
4.6 Principles of Classical and Quantum Radar as Hypothesis Testing . . . 63
4.6.1 Measurements: POVMs . . . 64
4.6.2 Joint vs. Independent Measurement . . . 64
4.6.3 Classical Radar Formulation . . . 64
4.6.4 Quantum Radar (Quantum Illumination) Formulation . . . 65
4.7 Resource Generation: Two-Mode Squeezed Vacuum (TMSV) . . . 65
4.8 Gaussian States, Quadratures, and Covariance Matrices . . . 66
4.8.1 Quadrature Representation . . . 66
4.8.2 Covariance Matrices Under Each Hypothesis . . . 66
4.8.3 Continuous Variables and Phase Space . . . 67
4.9 Operator-Level Derivation of Noise and Correlation Parameters . . . 68
4.9.1 Two-Mode Squeezing Transformation . . . 68

4.9.2 Quadrature Operators and Variances . . . 69
4.9.3 Connection to Mean Photon Number . . . 69
4.9.4 Beam-Splitter Channel at the Operator Level . . . 69
4.10 Quantum Chernoff Bound and the Emergence of the 6 dB Advantage . . . 70
4.10.1 Quantum Chernoff Bound . . . 70
4.10.2 Quantum Fidelity . . . 70
4.10.3 Helstrom Bound . . . 70
4.10.4 Determinant Structure and Correlation Contribution . . . 70
4.10.5 Derivation of the Quantum Error Exponent . . . 71
4.10.6 The 6 dB Advantage . . . 71
4.10.7 Interpretation . . . 72
4.11 Conclusion . . . 72

5 Simulation Results **73**
5.1 Introduction . . . 74
5.2 Interactive Radar-Oriented Demonstration of Quantum Advantage . . . 74
5.2.1 Simulation Configuration . . . 75
5.2.2 Influence of Radar Parameters . . . 76
5.2.3 Overall Interpretation . . . 76
5.3 Stage Two: Fock-Space Simulation . . . 77
5.3.1 Convergence in the Fock Truncation . . . 77
5.3.2 Computational Limitation . . . 78
5.3.3 Motivation for the Next Stage . . . 79
5.4 Gaussian-Covariance Simulation of Quantum Illumination . . . 79
5.4.1 Simulation Parameters . . . 80
5.4.2 ROC Curve Analysis . . . 80
5.4.3 Detection Advantage versus Transmissivity . . . 81
5.4.4 Computational Performance . . . 82
5.4.5 Overall Interpretation . . . 82
5.5 Agreement Between Methods . . . 83
5.5.1 Performance Evaluation and Results . . . 84
5.5.2 Interpretation of Results . . . 84
5.5.3 Conclusion of Numerical Analysis . . . 84
5.6 Bridging Radar Engineering and Quantum Illumination . . . 85
5.7 Conclusion . . . 87

6 Conclusion **88**
6.1 Key-points : . . . 89
6.2 Contribution : . . . 89
6.3 Future Work . . . 89

Bibliography **91**

List of Tables

2.1 Typical RCS values for different targets [1] 36
2.2 Standard radar frequency bands and typical applications 36
2.3 Summary of key radar parameters and typical values 41

4.1 Key parameters in quantum illumination and their typical regimes for the quantum advantage. 59

5.1 Convergence of the Fock-space simulation with truncation N_{HILBERT}. The energy error $\left| n_{\mathrm{out}} - (\eta N_S + (1-\eta) n_{\mathrm{th}}) \right|$ measures how closely the numerical channel reproduces the exact thermal-loss formula; μ_1 and σ_1 are the mean and standard deviation of the receiver observable C under H_1. 78
5.2 Approximate feasibility of the Fock-space simulation as a function of the background photon number N_{TH}, with the corresponding minimum truncation and two-mode state size. The cost becomes prohibitive well before reaching realistic background levels. 79

List of Figures

2.1 Block diagram of a basic monostatic pulse radar system. [2] 28
2.2 Comparison of isotropic and directional antenna radiation patterns. [3] . . . 30
2.3 Received Power vs Range 38
2.4 Effect of radar cross-section (RCS) on received power and detection range. . 39
2.5 Comprehensive analysis of radar cross-section (RCS) effects on received power and detection performance. 40

3.1 Theoretical ROC curves for a matched filter detector in AWGN at different SNR values. 53

4.1 Conceptual diagram of the Quantum Illumination protocol, showing the entangled source, signal transmission through the lossy thermal-noise channel, idler retention, and joint measurement for target detection. Adapted from [4]. 59

5.1 ROC curves (left panel) and quantum advantage ΔP_D (right panel) for the interactive radar demonstration. 75
5.2 ROC curves from the Fock-space simulation (quantum versus classical) at the chosen parameters. 77
5.3 ROC curves for quantum illumination (solid lines) versus classical coherent-state radar (dashed lines) at different transmissivities. 80
5.4 Quantum advantage at fixed false-alarm probability $P_{FA} = 0.1$ as a function of transmissivity η. 81

List of Acronyms

- **AWGN** : Additive White Gaussian Noise
- **AUC** : Area Under the Curve
- **CM** : Covariance Matrix
- **CV** : Continuous Variable
- **CW** : Continuous Wave
- **dB** : Decibel
- **FMCW** : Frequency-Modulated Continuous Wave
- **I/Q** : In-phase / Quadrature
- **IQSCC** : Integrated Quantum Sensing and Classical Communication
- **ISAC** : Integrated Sensing and Communication
- **JPA** : Josephson Parametric Amplifier
- **LRT** : Likelihood Ratio Test
- **OPA** : Optical Parametric Amplifier
- **POVM** : Positive Operator-Valued Measure
- **PRF** : Pulse Repetition Frequency
- **PRI** : Pulse Repetition Interval
- **QCB** : Quantum Chernoff Bound
- **QI** : Quantum Illumination
- **QTMS** : Quantum Two-Mode Squeezing
- **RADAR** : Radio Detection And Ranging
- **RCS** : Radar Cross Section
- **ROC** : Receiver Operating Characteristic
- **SNR** : Signal-to-Noise Ratio
- **SPDC** : Spontaneous Parametric Down-Conversion
- **TMSV** : Two-Mode Squeezed Vacuum

General Introduction

Project Context

Radar technology has been developing since the early 20th century and has proven its importance across a wide range of applications. While it is used in police and weather radars, the most prominent domain remains military applications. The race to develop better radar systems has never stopped, aiming to overcome various limitations and challenges such as environmental variations, thermal noise, stealth targets with low RCS, jamming, and the range drop-off. A radar is a complete system. When applied to detection, numerous techniques and algorithms emerge. Among them, the matched filter is particularly noteworthy. Although it represents the optimal detection framework, a new class of technologies and an entirely new framework emerged in the 21st century : quantum radars, and more precisely, quantum illumination. In theory, this new concept has been proven to perform significantly better in terms of detection error probability, particularly in low-signal, high-noise regimes, compared to classical radar. Yet no clear advancements have been made toward the realization of such technology.

Structure of the manuscript

The thesis is organized into six chapters, each building a solid understanding of core concepts and culminating in implementation and comparison.

Chapter 1 — Introduction and State of Art

Reviews research papers on quantum illumination, quantum radars, their possible applications, and related technologies.

Chapter 2 — Classical Radar Fundamentals

Derives and defines each radar concept intuitively.

Chapter 3 — Detection Theory

Explores detection theory, introduces the matched filter, and defines performance metrics.

Chapter 4 — Discovering Quantum Radars

Introduces the quantum mathematical foundations, explains the quantum illumination protocol, and derives the theoretical 6 dB advantage.

Chapter 5 — Simulation Results

Presents simulation results comparing classical and quantum detection across multiple stages and realistic radar parameters.

Chapter 6 — Conclusion

Concludes the findings, discusses limitations, and suggests future research directions.

Chapter 1

Introduction and State of the Art

In this Chapter, we provide a comprehensive introduction to the intersection of classical radar and quantum mechanics, establishing a foundation to bridge the gap between theoretical quantum science and practical engineering. We begin by outlining the two primary research axes of this thesis: addressing the fundamental detection limitations of classical matched filters in low-SNR regimes and developing a simulation framework to compare classical and quantum detection across realistic physical parameters. Following a historical review of radar evolution and quantum foundations like entanglement, we analyze the three main classes of quantum radar, identifying Quantum Illumination (QI) as the most resilient protocol for noisy environments. We explore the potential applications of these technologies in military counter-stealth, civilian aviation, and low-power biomedical sensing. Finally, we define the core research objectives.

- Definition.
- Problem statement.
- State of art.
- Motivation and research objectives.
- Contribution.

1.1 Definition

Radar is a technology that has been developed since the early twentieth century; the word is an abbreviation for RAdio Detection And Ranging. The fundamental role of a radar is detection: it transmits a signal, receives the echo, and correlates the transmitted waveform with the received one to judge whether the signal has reflected off a target. In essence, it answers a single question: is a target present? Radar performs this task well when the reflected signal is strong, but when the noise is high compared to the signal, it begins to struggle; in the weak-signal, high-noise regime, classical detection approaches its fundamental limits. This thesis examines a non-classical alternative: quantum radar, and specifically the quantum illumination protocol, which promises a lower error probability in this same hypothesis-testing problem. Our aim is to evaluate the effectiveness of this approach in radar-engineering terms.

1.2 Problem Statement

This thesis is structured around two major research axes that reflect both the diversity and complementarity of the subject.

First axis: Detection limitations

Classical optimal detection, based on the matched filter and detection theory, reaches a fundamental performance ceiling in low-SNR regimes. This limitation persists whether the challenge is overcoming jamming, detecting stealth targets with low RCS, or operating with low transmit power. Quantum illumination claims superior performance in these scenarios and the ability to counter stealth technologies. The objective of this axis is to model the quantum illumination framework and simulate it using its appropriate metrics.

Second axis: Frameworks comparison

While theoretical analysis is sufficient for ideal conditions, it does not account for realistic radar parameters nor clearly show how performance varies with each parameter. The objective of this axis is to simulate both classical and quantum frameworks across multiple varying parameters and compare them using their respective metrics. The thesis bridges the "theory-practice gap" that currently separates quantum information science from classical electrical engineering. While there is literature on both subjects, they are rarely combined into a comprehensive, multi-parameter engineering simulation framework.

The overall objective is to bridge the gap between written theory and performance analysis in radar engineering.

1.3 State of Art

This section reviews the key developments that led to the emergence of quantum illumination as a candidate for next-generation radar systems. The discussion begins with a brief history of classical radar, establishing the technological context and the persistent limitations that motivated alternative approaches. A concise history of quantum mechanics follows, highlighting the concepts of superposition and entanglement that later became central to quantum sensing. The chapter then traces the evolution of quantum radar concepts, from early proposals to the specific protocol of quantum illumination. Finally, current research directions and expected applications.

1.3.1 A Brief History of Radar

The development of radar spans more than a century. In 1904, Christian Hülsmeyer demonstrated a simple ship detection device using radio waves, but the system lacked range measurement capability. The modern era of radar began in the 1930s, with independent developments in several nations: Robert Watson-Watt led the construction of the Chain Home system in Britain, which proved decisive during the Battle of Britain; similar systems emerged in Germany, the United States, and the Soviet Union.
Post-World War II advances introduced monopulse tracking, moving target indication, and pulse compression. The invention of the maser and later the laser opened new frequency bands, but the fundamental detection limit remained thermal noise.
By the 1950s, the matched filter was established as the optimal linear detector for known signals in additive white Gaussian noise, a result that defines the classical performance ceiling against which all later proposals, including quantum illumination, are compared [5, 6]. Despite decades of engineering progress, classical radar faces fundamental limits: the received signal power decays as the fourth power of range, stealth technology reduces radar cross-section by orders of magnitude, and jamming can raise the noise floor arbitrarily. These persistent challenges motivated the search for detection strategies that go beyond classical signal processing.

1.3.1.1 Concept of Radar detection and Matched Filtering

Radar is an electromagnetic system for the detection and location of objects. It operates by transmitting a particular type of waveform, a pulse-modulated sine wave for example, and detects the nature of the echo signal. Radar is used to extend the capability of one's senses for observing the environment, especially the sense of vision. The value of radar lies not in being a substitute for the eye, but in doing what the eye cannot do. Radar cannot resolve detail as well as the eye, nor is it capable of recognizing the "color" of objects to the degree of sophistication of which the eye is capable. However, radar can be designed to see through

conditions impervious to normal human vision, such as darkness, haze, fog, rain, and snow. In addition, radar has the advantage of being able to measure the distance or range to the object [5].

A matched filter is designed to maximize the output peak signal-to-average noise (power) ratio. It has a frequency-response function proportional to the complex conjugate of the signal spectrum. The ideal matched-filter receiver cannot always be exactly realized in practice, but it is possible to approach it with practical receiver circuits. The output of a matched-filter receiver is the cross-correlation between the received waveform and a replica of the transmitted waveform. Hence it does not preserve the shape of the input waveform; there is no reason to preserve the shape as long as the output signal-to-noise ratio is maximized [7].

1.3.2 A Brief History of Quantum Mechanics

Quantum mechanics emerged in the early 20th century to explain phenomena that classical physics could not. In 1900, Max Planck introduced the concept of energy quantization to explain blackbody radiation. Albert Einstein's 1905 explanation of the photoelectric effect established that light consists of discrete quanta (photons). Niels Bohr's 1913 atomic model incorporated quantized energy levels, and Werner Heisenberg, Erwin Schrödinger, and Paul Dirac formulated the mathematical framework of matrix and wave mechanics between 1925 and 1926.

Two concepts from this framework are central to quantum radar. First, superposition allows a quantum system to exist in a linear combination of states, with measurement outcomes probabilistic. Second, entanglement described by Einstein, Podolsky, and Rosen in their 1935 paradox and formalized by John Bell in 1964 creates correlations between systems that have no classical analogue. Entangled particles remain correlated regardless of distance, a property that appears to violate local realism.

For decades, entanglement was considered a philosophical curiosity. The 1980s and 1990s saw the emergence of quantum information science, with proposals for quantum computing, quantum cryptography, and quantum metrology. Researchers realized that entanglement could be harnessed not just for computation but also for sensing, achieving precision beyond classical limits. This insight eventually led to the proposal of quantum illumination [8].

1.3.3 From Quantum Sensing to Quantum Illumination

By the early 2000s, quantum metrology had established a clear result: entanglement could improve measurement precision beyond classical limits in controlled laboratory settings. Quantum interferometry achieved the Heisenberg limit, and quantum lithography demonstrated sub-wavelength resolution. These successes led researchers to consider a natural

extension: could entanglement improve radar?

The initial consensus was pessimistic, radar operates in precisely the environment where quantum effects are known to fail : high thermal noise, strong loss, and decoherence. Entanglement is fragile, a single photon lost to the environment or a single noise photon corrupting the signal was thought to destroy any quantum advantage. Classical radar engineers, accustomed to decades of optimizing the matched filter, saw little reason to look at quantum mechanics. Seth Lloyd challenged this consensus in 2008 [9]. He asked a counterintuitive question: what if entanglement survives not in individual photons but in their statistical correlations? His quantum illumination proposal showed that even when the signal photon is embedded in bright thermal noise and most of the entanglement is destroyed, a joint measurement on the returned signal and the retained idler can still outperform any classical strategy of equal energy. The advantage is not large : 6 dB in the error exponent, but it persists precisely where classical radars fail : low reflectivity, high noise, low signal power.

The physics community received the proposal with interest mixed with skepticism. Subsequent work by Tan et al. (2008) [10] and Shapiro (2009) [11] placed quantum illumination on rigorous Gaussian-state foundations, confirming the 6 dB advantage. Experimental demonstrations followed, first in optical regimes [12], then at microwave frequencies (Barzanjeh et al., 2015).

The engineering community, however, remained cautious, quantum illumination's performance metrics, error probability and quantum Chernoff bound do not translate directly to radar engineering parameters such as detection probability, false alarm rate, and maximum range. A quantum advantage expressed in decibels of error exponent does not tell an engineer how much further a radar can see against a stealth target. This disconnect between theoretical proof and engineering utility is the central motivation for this thesis: to bridge the gap by translating quantum illumination into radar language [13].

1.3.4 Quantum Radar: Principles and Classes

A quantum radar is based on physical phenomena described by quantum physics, not solely by classical physics. As in many other emerging quantum technologies like quantum computing and quantum communication, entanglement is the central phenomenon used in quantum radar. Entanglement implies a strong correlation between two or more particles (photons, pulses). Entanglement persists even when the particles are separated by distance.

According to Luong et al. [14], three classes of quantum radars are discussed in literature : quantum interferometric radar, QTMS radar, and quantum illumination.

- **Quantum Interferometric Radar :**

  Quantum interferometry is much like normal interferometry, except that a quantum signal generator produces an entangled quantum state called a N00N state. Its main challenges are the difficulty of generating N00N states and their fragility, resulting in restricted practical application.

- **QTMS Radar :**

QTMS (Quantum Two-Mode Squeezing) radar is a simplified version of quantum illumination that, conceptually, comes closer to conventional radar. It uses an entangled signal generator, but the receiver setup is entirely conventional: instead of a complicated joint measurement, heterodyne measurements are performed. Its main challenge is the requirement of cryogenic refrigeration.

- **Quantum Illumination :**

  The most promising quantum radar technique today appears to be quantum illumination, theoretically introduced by Seth Lloyd in 2008 [9]. Two entangled photons are generated: the idler is kept at the radar, while the signal is sent toward the target. If the signal photon is reflected back to the radar, it is likely to be detected due to its strong correlation with the idler.

  In the QI strategy, a pair of entangled signal and idler photons illuminates the target. The signal is transmitted to probe the environment, while the idler is retained until the signal returns. Finally, a joint measurement on the returning signal together with the retained idler distinguishes the signal photons from thermal noise [9, 10].

  Unlike many other quantum technologies, quantum illumination works even in noisy environments. Therefore, the quantum illumination protocol has also been proposed for quantum communication. Its main challenges are twofold: generating an appropriate entangled signal and implementing the joint measurement.

Theoretical Status

The theoretical status of quantum illumination is more nuanced than a simple 6 dB advantage. Shapiro, in his retrospective account [11], notes that Lloyd's original 2008 comparison was between entangled and unentangled strategies, not necessarily against the optimal classical radar. Subsequent work by Shapiro and Lloyd (2009) and Tan et al. (2008) corrected this by comparing Gaussian-state quantum illumination against coherent-state classical radar, the latter being optimal among all classical schemes for the same average transmitted photon number.

The regime where QI shows advantage is precisely the challenging one: low reflectivity ($0 < \kappa \ll 1$), low signal brightness ($N_S \ll 1$), high thermal noise ($N_B \gg 1$), and many temporal modes ($M \gg 1$). Coherent-state classical radar has an error exponent of $\kappa N_S/(4N_B)$, while QI achieves $\kappa N_S/N_B$, a factor of four (6 dB) improvement. However, the advantage only manifests when κN_S is sufficiently large relative to N_B/M; otherwise, performance is identical.

Shapiro also notes that some subsequent research "took much of the air out of QI's balloon," tempering early hype. Yet QI remains significant as the first example of a bosonic system that offers performance improvement on an entanglement-breaking channel. The lesson is not that entanglement is magic, but that its statistical remnants can be exploited even when individual quantum correlations are destroyed by loss and noise.

1.3.4.1 Optimal vs. Implementable Receivers

The 6 dB advantage derived above is an upper bound: it is the gain of the *optimal* joint measurement on the returned signal and the retained idler, the receiver that saturates the quantum Chernoff bound. No physical realization of this optimal receiver is currently known. Guha and Erkmen [15] addressed this gap by proposing two structured receivers that can actually be built, an optical parametric amplifier (OPA) receiver and a phase-conjugation receiver and showed that each recovers up to half of the optimal gain, that is, about 3 dB over the optimal classical strategy. These receivers extract the residual signal–idler correlation through a single feasible nonlinear interaction rather than an idealized joint measurement.

This distinction is central to the present work. The correlation observable we simulate, $C = X_s X_i - P_s P_i$, belongs to this implementable (OPA/phase-conjugation) family rather than to the optimal class. Accordingly, while we acknowledge that the optimal receiver provides the full 6 dB gain, we also note that the implementable receiver achieves around 3 dB; it is this implementable class that we simulate throughout this thesis.

1.3.5 Applications of Quantum Radar

- **Military and Detection Applications:**

  The most headline-grabbing application of quantum radar is undoubtedly in the military domain, particularly for counter-stealth and advanced threat detection. Modern stealth aircraft like the F-35 or B-2 bomber are designed to evade classical radars by having a minuscule radar cross-section, reflecting away or absorbing much of the incident radar energy. A sufficiently sensitive quantum radar could flip this script. Because it can separate a target's weak echo from overwhelming background noise, a quantum radar theoretically might detect even a "nearly invisible" stealth plane.

- **Civilian Applications:**

  While defense gets the spotlight, quantum radar (and quantum illumination techniques) could have a variety of non-military applications as well. One oft-mentioned use is in air traffic control and aviation safety. A quantum radar system could potentially monitor civilian airspace with much lower power emissions, which means less interference with other systems and reduced radiation exposure. It might detect small objects like hobby drones or birds near airports that conventional radars have trouble picking out from ground clutter. Because a quantum radar can work in very noisy conditions, it could be useful in busy urban environments where there's a lot of electromagnetic noise or multipath reflections. Imagine an air traffic control radar that can see a small quadcopter hovering near a runway despite the radar confusion caused by buildings, weather, and other aircraft, quantum-enhanced sensing might help achieve that level of fidelity.

- **Biomedical Applications:**

  Quantum radars appear naturally suited to medical applications, as they possess many desirable properties: they transmit only non-ionizing radiation at extremely low signal powers, and they are unlikely to interfere with other medical equipment [16]. The viability of quantum interferometry for biomedical applications is further discussed in [17].

- **Communication Applications**

  Beyond dedicated radar systems, quantum illumination has been proposed for integrated sensing and communication. Alsaui et al. (2025)[18] introduced the concept of IQSCC (Integrated Quantum Sensing and Classical Communication), where a 6G base station performs quantum illumination radar while simultaneously communicating with users. The same entangled signal used for target detection also carries classical information. The advantage is two-fold: the quantum radar operates at very low power, minimizing interference with communication, and the existing communication infrastructure reduces the hardware burden for quantum sensing deployment. This approach remains theoretical but highlights a promising direction for future wireless networks.

1.4 Motivation and research Objectives

1.4.1 Motivation

This thesis is motivated by three core objectives :

- To understand the fundamentals of classical radar and the theoretical foundations of quantum illumination.
- To develop a simulation framework that explores both classical and quantum detection.
- To compare their performance across one of the different parameters (range, RCS, noise) and assess the quantum advantage.

1.4.2 Research objectives

This thesis is theory-heavy, as the modeling and comparison of classical and quantum detection stand on mathematical foundations and deep theoretical understanding. Throughout this work, we will:

- Derive, explain, and simulate classical radar and detection concepts (radar equation, RCS, noise, matched filter).
- Understand the formal framework of binary hypothesis testing such as Neyman-Pearson and ROC curves.
- Introduce the quantum foundations needed for this work : TMSV states, Gaussian states, covariance matrices.

- Derive, explain, and implement quantum illumination simulation with relevant concepts : lossy channel, quantum Chernoff bound, Helstrom bound.
- Compare classical vs quantum performance under identical physical parameters : range, RCS, noise, transmitted power.
- Understand how their parameters overlap and identify regimes where each framework has a significant advantage.

1.5 Contribution

While theoretical proofs of the 6 dB quantum advantage are well established, existing research does not map quantum illumination parameters (transmissivity κ, noise photon number N_B, signal photon number N_S) to physical radar quantities (range R, radar cross-section σ, transmit power P_t). Consequently, performance predictions remain abstract and inaccessible to radar engineers.

This thesis bridges this gap by developing a simulation framework that translates classical radar parameters into quantum inputs, enabling direct comparison of detection probability and error probability under identical physical conditions. The contribution is a quantitative assessment of quantum illumination's advantage for realistic radar scenarios.

A further outcome of this mapping is interpretive. The 6 dB figure is often read as the ability to "detect the undetectable," but the advantage is more accurately an improvement in detection *efficiency* ,a multiplicative gain on the signal-to-noise ratio rather than a way to overcome the radar-equation losses that bound detection in the first place. By expressing the comparison in engineering terms, this thesis quantifies that distinction and identifies the regimes in which the quantum advantage is, and is not, operationally accessible.

Chapter 2

Classical Radar Fundamentals

In this chapter, we establish the physical and mathematical foundations of classical radar detection, creating an essential baseline to evaluate quantum illumination in later chapters. We outline fundamental radar measurements and explain how target range is calculated via round-trip time delay ($R = \frac{c \cdot \Delta t}{2}$), radial velocity is derived from the Doppler frequency shift, and angular direction is determined by electronic or mechanical antenna pointing. We detail the step-by-step derivation of the classical monostatic radar equation, demonstrating that the received signal power (P_r) decreases exponentially with the fourth power of range ($1/R^4$) due to spherical spreading losses. This fourth-root scaling law ($R_{\max} \propto \sigma^{1/4}$) imposes severe hardware demands, meaning that doubling a radar's range requires a 16-fold increase in transmit power or antenna size. We define the fundamental limits of detection by evaluating how thermal noise (Johnson-Nyquist noise) and the receiver noise figure combine to establish the minimum detectable signal ($S_{\min}$). Furthermore, we analyze structural variations, contrasting traditional monostatic architectures with bistatic and multistatic radar configurations. We explore systemic radar losses including plumbing, beamshape, and operational degradation and introduce the concept of Radar Cross Section (RCS). We explain that RCS represents a target's intrinsic electromagnetic reflectivity rather than its physical geometric size, illustrating why low-RCS stealth platforms drastically curtail classical detection ranges. Finally, we present simulation results to visually validate the severe impact of $1/R^4$ power decay, demonstrating how low-SNR regimes motivate the transition to advanced quantum sensing techniques.

- Introduction.
- Extraction of Radar measures.
- Derivation of Radar equation.
- Noise and minimum detectable signal.
- Maximum range equation.
- Monostatic, bistatic structures.

- Target localization.
- Radar cross section : Mathematically and conceptually.
- Power decay and effect of RCS on detection range.
- Conclusion.

2.1 Introduction

The term RADAR is an acronym that stands for RAdio Detection And Ranging. The primary purpose of a radar system is to determine the presence or absence of a target, along with its location and velocity. It achieves this by transmitting a high-power electromagnetic signal, receiving the reflected signal (or echo) from the target, and analyzing the characteristics of that received return.

2.2 What Radar Measures

Conceptual Explanation The radar is created to know the presence/absence of a target, its location, and its velocity. It works by sending a power signal then receiving it and judging the received signal. We can distinguish two types of radars, continuous wave radar, and pulse radar.

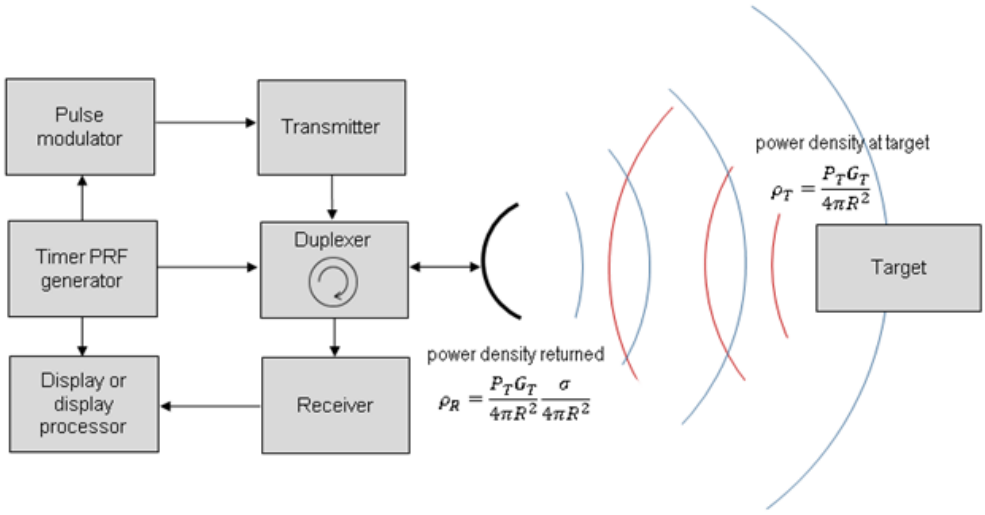

Figure 2.1: Block diagram of a basic monostatic pulse radar system. [2]

While pulse radar is the focus of this thesis, continuous wave (CW) radar represents an important alternative. CW radar transmits a constant frequency signal and extracts velocity from the Doppler shift, but cannot measure range directly without frequency modulation. Frequency-modulated CW (FMCW) radar allows both range and velocity measurement by transmitting a chirped signal. Military radars typically use pulse-based systems for long-range detection and unambiguous range measurement, which is why this thesis concentrates on pulse radar.

Mathematical Formulation Radar determines target parameters through three fundamental measurements:

Range : The radar transmits a pulse and measures the time delay Δt between transmission and reception of the echo. The range R is given by:

$$R = \frac{c \cdot \Delta t}{2} \tag{2.1}$$

where $c = 3 \times 10^8\,\text{m/s}$ is the speed of light. The factor $1/2$ accounts for the round trip.

Radial Velocity : Relative motion between the radar and the target induces a Doppler frequency shift f_d in the received signal. For a target moving with radial velocity v_r:

$$f_d = \frac{2v_r}{\lambda} \tag{2.2}$$

where λ is the wavelength. The velocity is then:

$$v_r = \frac{f_d \lambda}{2} \tag{2.3}$$

Angle : The direction (azimuth and elevation) of a target is determined by the antenna's pointing direction. In modern phased array radars, the beam is steered electronically by adjusting the phase shift between adjacent elements. The angle θ relative to boresight is related to the phase difference $\Delta\phi$ between elements spaced by distance d:

$$\Delta\phi = \frac{2\pi d}{\lambda} \sin\theta \tag{2.4}$$

More sophisticated techniques, such as monopulse processing, compare signals from multiple overlapping beams to achieve fine angular resolution.

CW Radars: A continuous wave radar is a type of radar system that transmits a known stable frequency continuously; it is received continuously by the radar. For a non-moving target, the signal is reflected then received at a similar frequency as the one transmitted. For a moving target, we have a Doppler shift: if the target is moving toward the radar, the received frequency is higher ; if the target is moving away, the received frequency is lower. The beat frequency is the subtraction of the two frequencies (transmitted and received); it is the frequency at which the two signals get "in phase".

Using the beat frequency, we can determine the speed of the object but not the direction, because the beat frequency would be the same whether the frequency difference is $+f_0$ or $-f_0$. To know the direction, we must send two signals, called I/Q signals (In phase and Quadrature, with a 90-degree phase shift between them). After mixing the transmitted and received signals, the in-phase component does not change regardless of whether the shift is $+f_0$ or $-f_0$, but the quadrature component does. By checking which of the two signals is leading in phase, we can determine direction. The beat frequency is proportional to the radial velocity of the object.

Frequency modulation can be used to obtain range. Distance does not cause a Doppler shift like velocity does; instead, it causes a time shift. Because of the time it takes for the

signal to travel to the object and back, the farther the object, the more time it takes. With a fixed-frequency signal, we cannot detect this delay because there is no pulse or defining characteristic to measure time; a delay of one period looks the same as two periods, three, and so on.

If we use a signal whose frequency is modulated in a triangular way (increasing and then decreasing over intervals), we can obtain two beat frequencies. If both beat frequencies are due to a time shift, one would be negative and the other positive; they would cancel out, confirming a Doppler shift. If both beat frequencies are Doppler-shifted (one negative, the other positive), they cancel out, confirming a time shift, meaning the object is not moving. Even if the signal experiences both Doppler and time shifts, having two beat frequencies allows us to separate the two contributions.

2.3 The Radar Equation Derivation

An isotropic antenna transmits power equally in all directions, distributing the power uniformly over the surface of a sphere. The power density at a distance R is given by:

$$\frac{P_t}{4\pi R^2} \tag{2.5}$$

A directive antenna concentrates more power toward a specific angle, and this increase is represented by the antenna gain G. The power density at distance R becomes:

$$\frac{P_t G}{4\pi R^2} \tag{2.6}$$

The antenna gain G is related to the effective aperture A_e and wavelength λ by:

$$G = \frac{4\pi A_e}{\lambda^2} \tag{2.7}$$

Intuitively, an isotropic radiator radiates equally in all directions (area $4\pi R^2$). A high-gain antenna is like a flashlight: it does not create new power but pinches the energy into a narrow beam. The effective aperture A_e is the "size of the bucket" capturing or directing waves. The λ^2 term reflects the diffraction limit: shorter wavelengths allow tighter focusing. By reciprocity, the same gain applies to both transmission and reception.

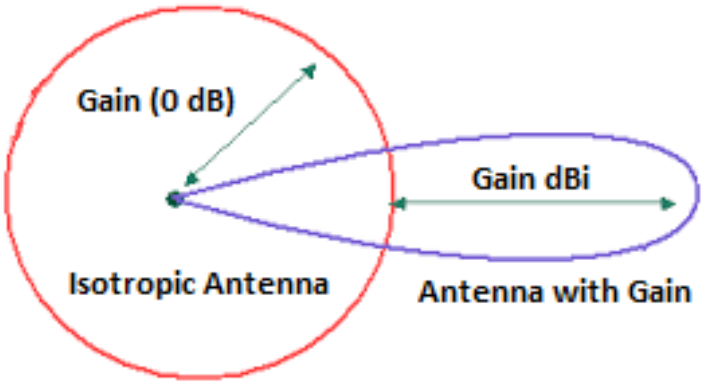

Figure 2.2: Comparison of isotropic and directional antenna radiation patterns. [3]

The signal illuminates a target with radar cross-section σ. The power intercepted by the target is the incident power density multiplied by the cross-section area. This power is then reradiated isotropically back toward the radar. Upon return, the power density at the radar is further reduced by spherical spreading, yielding:

$$\frac{P_t G \sigma}{(4\pi R^2)^2} = \frac{P_t G \sigma}{16\pi^2 R^4} \tag{2.8}$$

The receiving antenna has an effective aperture A_e, which captures a portion of the returned power density. Multiplying the power density at the radar by this effective area gives the received power [5, 19]:

$$P_r = \frac{P_t G \sigma A_e}{(4\pi R^2)^2} = \frac{P_t G \sigma A_e}{16\pi^2 R^4} \tag{2.9}$$

We note that the round-trip transmissivity used in the quantum comparison, η, is exactly this received-to-transmitted power ratio:

$$\eta = \frac{P_r}{P_t} = \frac{G^2 \lambda^2 \sigma}{(4\pi)^3 R^4 L}. \tag{2.10}$$

2.4 Noise and the Minimum Detectable Signal

The fundamental limit to radar detection is thermal noise, also known as Johnson-Nyquist noise. Any resistive element at temperature T generates random electromagnetic fluctuations. The available noise power is [5]:

$$P_n = kTB \tag{2.11}$$

where $k = 1.38 \times 10^{-23}\,\mathrm{J/K}$ is Boltzmann's constant, T is the absolute temperature in Kelvin, and B is the receiver bandwidth in Hz.

Real receivers add additional noise beyond thermal noise. This is quantified by the noise figure F, defined as the ratio of the actual output noise power to the output noise power of an ideal receiver with the same gain. The effective noise power at the receiver input becomes:

$$P_n = kTBF \tag{2.12}$$

For a signal to be reliably detected, its power must exceed the noise power by a sufficient margin. The minimum detectable signal $S_{\min}$ is therefore:

$$S_{\min} = kTBF\,(\mathrm{SNR})_{\min} \tag{2.13}$$

The term $(\text{SNR})_{\min}$ is the minimum signal-to-noise ratio required for detection. Typical values range from 10 to 13 dB, depending on the desired probability of detection and false alarm rate. A higher $(\text{SNR})_{\min}$ yields more reliable detection but reduces maximum range.

The limit of detection occurs when the received power equals the minimum detectable signal:

$$P_r = S_{\min} \tag{2.14}$$

For a typical radar at room temperature ($T = 290\,\text{K}$), bandwidth $B = 1\,\text{MHz}$, and noise figure $F = 3$ (5 dB), the noise power is approximately:

$$P_n = (1.38 \times 10^{-23}) \times 290 \times 1 \times 10^6 \times 3 \approx 1.2 \times 10^{-14}\,\text{W}\ (-139\,\text{dBW})$$

This is the floor below which signals cannot be reliably detected.

2.5 Maximum Range Equation

Setting the received power equal to the minimum detectable signal and solving for range gives the maximum detection range:

$$R_{\max} = \left(\frac{P_t G \sigma A_e}{(4\pi)^2 S_{\min}} \right)^{1/4} \tag{2.15}$$

This is the radar equation solved for range. Several observations follow directly:

- **Fourth-root dependence:** Doubling the maximum range requires increasing transmitted power, gain, or aperture by a factor of 16, or reducing the minimum detectable signal by the same factor. This is why extending radar range is difficult.
- **Target RCS scaling:** Increasing target RCS by a factor of 16 also doubles $R_{\max}$. This explains why stealth targets (very small σ) have dramatically reduced detection ranges.
- **Wavelength dependence:** Using the relation $G = 4\pi A_e/\lambda^2$, the equation can be rewritten in terms of G alone:

  $$R_{\max} = \left(\frac{P_t G^2 \lambda^2 \sigma}{(4\pi)^3 S_{\min}} \right)^{1/4} \tag{2.16}$$

  This form shows that for a fixed gain, longer wavelengths (smaller λ) reduce range, while for a fixed aperture, longer wavelengths also reduce range because A_e is fixed but gain drops.

The gain G is related to the effective aperture A_e and wavelength λ by:

$$G = \frac{4\pi A_e}{\lambda^2} \tag{2.17}$$

A larger effective aperture or smaller wavelength results in higher gain. Conversely, A_e must be sufficiently large when λ is large to capture the full wavefront pattern. Depending on the application, either G or A_e can be substituted into the radar equation as needed.

The fourth-root dependence makes radar range extension extremely challenging. To double the range of an existing radar, the transmitter power must be increased 16-fold, or the antenna area must be increased 16-fold, or the noise figure must be reduced by a factor of 16. In practice, most radar designs operate near the limits of what is technologically feasible for their size, weight, and power constraints.

2.6 Monostatic vs Bistatic Radar

- **Monostatic Radar**: a radar in which a common antenna is used for both transmission and reception. This is the most common configuration, as it simplifies the system and ensures alignment between transmitted and received beams.
- **Bistatic Radar**: employs separate antennas for transmission and reception, with a considerable distance between them. The receiver can be passive, making it harder to detect and jam. However, synchronization between transmitter and receiver is more complex.
- **Multistatic Radar**: consists of multiple receivers and a single transmitter, distributed over an area. This configuration provides multiple viewing angles, improving detection of stealth targets.

Bistatic and multistatic radars are relevant to quantum illumination because the idler is retained at the transmitter while the signal is received separately, so it's a form of quantum bistatic system. This thesis focuses primarily on monostatic radar for classical comparisons, but the quantum illumination protocol inherently employs a bistatic architecture.

We must note that QI is inherently bistatic in this sense: the idler is retained at the transmitter while only the signal is sent and received, so the protocol intrinsically separates the reference arm from the probe arm, much like a bistatic architecture separates transmitter and receiver.

2.7 Radar Losses

- **Plumbing Loss**: losses in transmission lines between the output of the transmitter and the antenna

- **Beamshape Loss**: only the center of the beam hits the target with maximum gain; the rest of the beam experiences reduced gain
- **Limiting Loss**: limiters are circuits that protect sensitive components of the receiver, introducing signal distortion and loss
- **Collapsing Loss**: added noise to an established SNR; can occur when collapsing 3D data to 2D or high-range resolution (HRR) to low-range resolution (LRR)
- **Operator Loss**: the operator is a human, introducing variability, reaction time delays, and decision errors
- **Non-ideal Equipment**: real-world hardware imperfections and component tolerances
- **Field Degradation**: performance deterioration due to environmental conditions, aging, and operational wear

These losses are collectively accounted for by the factor L in the radar equation, typically ranging from 2 to 10 (3 to 10 dB) depending on the system and environment.

2.8 Locating a Target

To locate a target, both distance and angle are required. In a bistatic radar configuration, the transmitter and receiver are separated by a known baseline distance D_b. The target is located at distances D_t (from transmitter) and D_r (from receiver), with angle Ψ_0 measured at the receiver.

The total path length is $S = D_t + D_r$. From the law of cosines:

$$D_t^2 = D_r^2 + D_b^2 - 2D_r D_b \cos(\Psi_0) \tag{2.18}$$

Since D_b is known and S is measured via time delay, D_r can be solved:

$$D_r = \frac{S^2 - D_b^2}{2(S - D_b \cos(\Psi_0))} \tag{2.19}$$

Doppler Beat Frequency. The radial velocity of the target is obtained from the Doppler frequency shift:

$$f_d = \frac{1}{\lambda} \left| \frac{d}{dt}(D_t + D_r) \right| \tag{2.20}$$

Pulse Repetition Frequency. The number of pulses transmitted per second is the pulse repetition frequency:

$$\text{PRF} = \frac{1}{\text{PRI}} \tag{2.21}$$

where PRI is the pulse repetition interval.

Maximum Unambiguous Range. To avoid range ambiguity, the next pulse is not transmitted until the echo from the farthest target returns. The maximum unambiguous range is:

$$R_{\text{unamb}} = \frac{c}{2 \cdot \text{PRF}} \tag{2.22}$$

If a target lies beyond this range, its echo arrives after the next pulse is sent, appearing closer than it actually is.

2.9 Radar Cross Section (RCS)

Radar Cross Section (RCS) is the effective area a perfect isotropic reflector would need to return the same power as the actual target. Despite its name, the RCS is not the physical cross-sectional area of the target. For example, a stealth fighter may have a physical cross-section of $10\,\text{m}^2$ but an RCS of only $0.0005\,\text{m}^2$ [1].
The RCS is formally defined as [5]:

$$\sigma = \lim_{R \to \infty} 4\pi R^2 \cdot \frac{|E_s|^2}{|E_i|^2} \tag{2.23}$$

where E_i is the incident electric field strength and E_s is the scattered field strength measured at distance R from the target.

To provide intuition, consider a sphere acting as an isotropic scatterer. The transmitted power illuminates the sphere, and the scattered power is distributed uniformly over a sphere of radius R. The RCS is derived by equating the backscattered power from the actual target to that from a hypothetical isotropic reflector. Since measurements are conducted in the far-field region, the limit $R \to \infty$ ensures that the RCS is independent of range.

Notably, σ is independent of the measurement distance. As R increases, $|E_s|^2$ decays as $1/R^2$ due to spherical spreading. Multiplying by $4\pi R^2$ cancels this dependence, making σ an intrinsic property of the target rather than a function of measurement distance.

A large RCS results in a high signal-to-noise ratio (SNR), thus enabling better detection. Conversely, a small RCS yields a low SNR, which enhances stealth capabilities.

Quantum illumination claims a distinct advantage precisely in the low RCS / low SNR regime where classical radar fails. Therefore, comparing performance relative to RCS will be useful to benchmark quantum enhancement.

Table 2.1: Typical RCS values for different targets [1]

Target	**RCS (m^2)**
Stealth fighter (F-35)	0.001 - 0.01
Bird	0.01
Small UAV	0.1
Fighter jet (non-stealth)	5 - 10
Large aircraft (Boeing 747)	100
Ship	10,000+

2.10 Radar Frequency Bands

Radar systems operate across a wide range of frequencies, each with distinct propagation characteristics, resolution capabilities, and application domains. Lower frequencies (HF, VHF, UHF) penetrate weather and foliage more effectively and are used for long-range surveillance and over-the-horizon radar, but they suffer from poor resolution. Higher frequencies (X, Ku, Ka bands) provide finer resolution and smaller antenna sizes for the same gain, making them suitable for fire control, imaging, and automotive radar, but they experience higher atmospheric attenuation, particularly in rain. The choice of frequency band involves trade-offs between range, resolution, atmospheric losses, and antenna size. Table 2.2 summarizes the standard radar frequency bands and their typical applications.

Table 2.2: Standard radar frequency bands and typical applications

Band	**Frequency**	**Wavelength**	**Typical Use**
HF	3-30 MHz	10-100 m	Over-the-horizon radar
VHF	30-300 MHz	1-10 m	Early warning, air traffic
UHF	300-1000 MHz	0.3-1 m	Surveillance, counter-stealth
L	1-2 GHz	15-30 cm	Air traffic control, surveillance
S	2-4 GHz	7.5-15 cm	Weather radar, maritime
C	4-8 GHz	3.7-7.5 cm	Long-range tracking
X	8-12 GHz	2.5-3.7 cm	Fighter radar, fire control
Ku	12-18 GHz	1.7-2.5 cm	Satellite communication
K	18-27 GHz	1.1-1.7 cm	Radar altimetry
Ka	27-40 GHz	0.75-1.1 cm	High-resolution imaging
W	75-110 GHz	2.7-4 mm	Millimeter-wave radar

2.11 Simulations

Range of Radar Figure 2.3 illustrates the variation of the received power as a function of range based on the classical monostatic radar equation. The simulation is performed using a transmit power of $P_t = 1$ MW, antenna gain $G = 30$ dB, wavelength $\lambda = 0.03$ m (corresponding to a 10 GHz carrier), and a target radar cross-section $\sigma = 1$ m^2. System losses are modeled by a factor $L = 2$. The receiver noise floor is computed as $S_{\min} = kT_0BF_n \cdot \mathrm{SNR}_{\min}$, assuming a bandwidth $B = 1$ MHz, noise figure $F_n = 5$ dB, and a minimum detection threshold $\mathrm{SNR}_{\min} = 10$ dB.

The first subplot (linear scale) highlights the rapid decay of the received power with distance, reflecting the R^{-4} dependence of the radar equation. This strong attenuation is further confirmed in the log-log representation, where the received power follows a straight line, consistent with the theoretical power-law behavior. The semi-logarithmic plot, commonly used in radar engineering, provides a more practical visualization by expressing power in decibels, allowing a clearer comparison with the receiver sensitivity.

By introducing the noise floor, the maximum detection range is identified as the intersection between the received power curve and the minimum detectable signal. For the chosen parameters, this limit is found to be approximately $R_{\max} \approx 36.9$ km. The shaded region represents the operational detection zone, where the received signal exceeds the noise threshold and detection is theoretically possible. Beyond this range, the signal-to-noise ratio falls below the required threshold, making reliable detection unlikely.

These results emphasize that radar performance is fundamentally constrained by propagation losses and thermal noise. In particular, the R^{-4} dependence imposes a severe limitation on long-range detection, motivating the need for advanced techniques to improve sensitivity in low-SNR regimes. This observation provides a basis for the comparative analysis with quantum illumination presented in the following chapters.

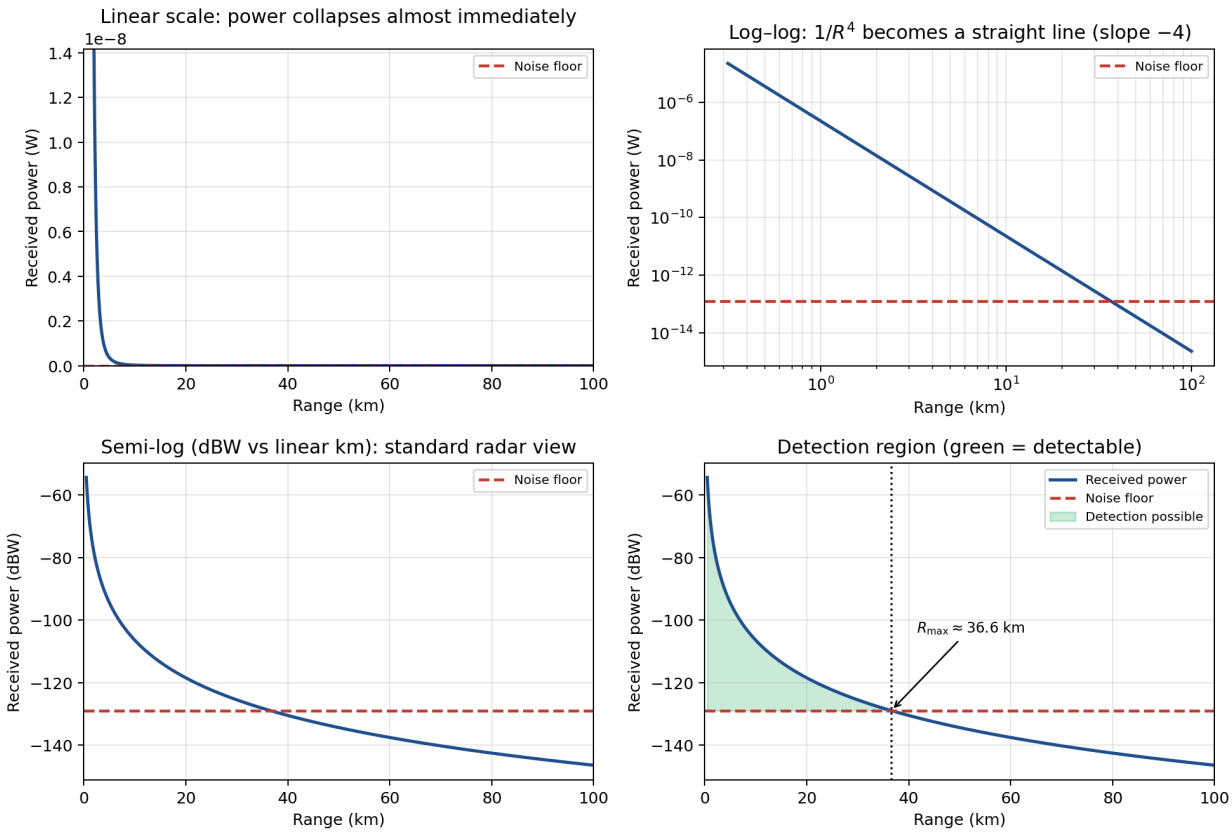

Figure 2.3: Received Power vs Range

RCS effect on Range Figure 2.4 shows the impact of the radar cross-section (RCS) on the received power as a function of range. Several target scenarios are considered, with σ varying from 0.1 m^2 to 100 m^2. As predicted by the radar equation, the received power scales linearly with the RCS, which translates into a constant vertical shift in the logarithmic (dB) domain. In particular, each decade increase in σ results in an approximate 10 dB increase in received power, while preserving the same slope associated with the R^{-4} propagation loss.

The intersection of each curve with the noise floor defines the corresponding maximum detection range. It is observed that increasing the RCS significantly extends the detection distance: low-reflectivity targets quickly fall below the detection threshold, whereas highly reflective targets remain detectable over much longer ranges. This illustrates that, although the dependence on σ is linear in power, it leads to a nonlinear improvement in detection range, which is a critical factor in radar performance analysis.

These results highlight the inherent limitations of classical radar systems when dealing with low-RCS targets, particularly in noisy environments. Such scenarios are of practical importance in applications involving stealth or weakly reflecting objects, and they further motivate the investigation of advanced detection strategies, including quantum illumination, which aim to improve sensitivity under low signal-to-noise ratio conditions.

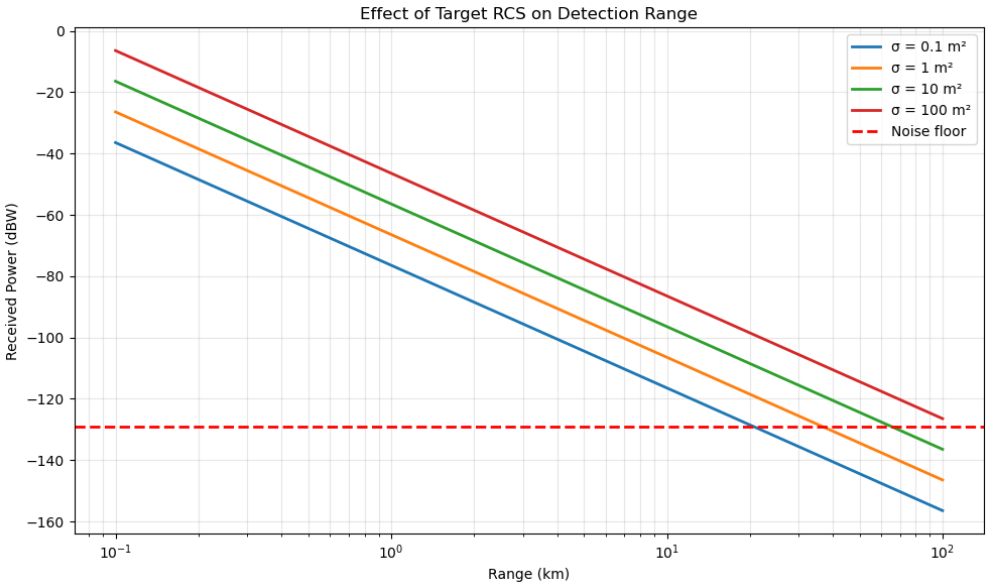

Figure 2.4: Effect of radar cross-section (RCS) on received power and detection range.

RCS Range Analysis : Figure 2.5 presents a comprehensive analysis of the impact of radar cross-section (RCS) on received power and detection performance across multiple target classes, ranging from stealth platforms ($\sigma \approx 10^{-3}$ m^2) to large maritime targets ($\sigma \approx 10^4$ m^2). The simulations are based on the classical monostatic radar equation using a transmit power of $P_t = 1$ MW, antenna gain $G = 30$ dB, wavelength $\lambda = 0.03$ m, and system losses $L = 2$. The receiver sensitivity is determined by a thermal noise model $S_{\min} = kT_0BF_n \cdot \mathrm{SNR}_{\min}$ with $B = 1$ MHz, $F_n = 5$ dB, and $\mathrm{SNR}_{\min} = 10$ dB.

Power vs Range: The upper subplots illustrate the received power as a function of range for different RCS values using both semi-logarithmic and log-log representations. All curves exhibit identical slopes, confirming the R^{-4} dependence imposed by the radar equation. Variations in RCS result in a constant vertical shift in the decibel domain, with each decade increase in σ producing an approximate 10 dB gain in received power. This behavior highlights that target reflectivity directly affects signal strength without altering propagation characteristics.

Detection Range Scaling: The relationship between maximum detection range and RCS is explicitly shown in the lower-left subplot. The results closely follow the theoretical scaling law $R_{\max} \propto \sigma^{1/4}$, as indicated by the reference dashed line. This implies that large variations in RCS translate into relatively modest changes in detection range. For example, increasing the RCS by four orders of magnitude results in only a one-order-of-magnitude increase in detectable distance. This sublinear scaling constitutes a fundamental limitation of classical radar systems, particularly in the detection of low-RCS targets.

Detection Regions: The lower-right subplot provides a visualization of the detection regions for selected target types by comparing the received power with the noise floor. The

shaded areas indicate ranges where the signal-to-noise ratio exceeds the detection threshold. It is observed that stealth targets become undetectable at relatively short distances, whereas conventional and large targets remain detectable over significantly longer ranges. This clearly demonstrates the strong dependence of operational detection capability on target reflectivity and highlights the vulnerability of classical radar systems in low-RCS scenarios.

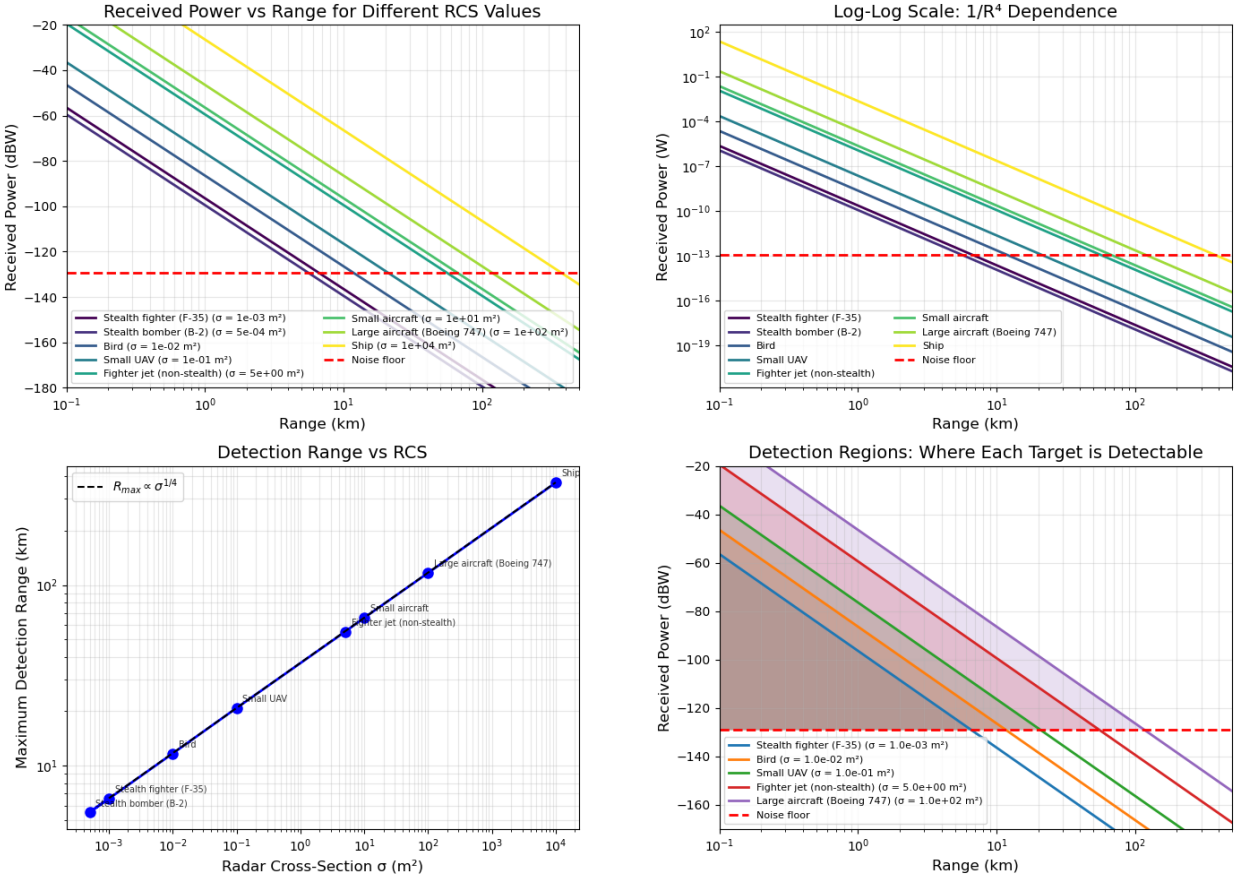

Figure 2.5: Comprehensive analysis of radar cross-section (RCS) effects on received power and detection performance.

2.11.1 Summary of Key Radar Parameters

Table 2.3: Summary of key radar parameters and typical values

Parameter	**Symbol**	**Typical Range**
Transmit power	P_t	1 kW - 10 MW
Antenna gain	G	20 - 50 dB
Wavelength	λ	0.01 - 1 m
Radar cross-section	σ	0.001 - 1,000 m^2
Range	R	1 - 500 km
Noise figure	F	2 - 10 (3 - 10 dB)
Bandwidth	B	100 kHz - 100 MHz
Pulse repetition frequency	PRF	30 kHz - 100 kHz

2.12 Conclusion

This chapter established the physical and mathematical foundations of classical radar. The key results are:

- The radar equation $P_r = P_t G^2 \lambda^2 \sigma / ((4\pi)^3 R^4 L)$ shows that received power decays as $1/R^4$, making long-range detection fundamentally challenging.
- Thermal noise sets the minimum detectable signal $S_{\min} = kTBF(\text{SNR})_{\min}$.
- Maximum detection range scales as $R_{\max} \propto \sigma^{1/4}$, meaning stealth targets with 100× smaller RCS are detected at about 1/3 the range.
- Radar cross-section is an intrinsic target property, not physical area, and determines how much power is reflected back.
- System losses (plumbing, beamshape, limiting, etc.) are collectively accounted for by the loss factor L.
- Range ambiguity is determined by pulse repetition frequency: $R_{\text{unamb}} = c/(2 \cdot \text{PRF})$.

These classical results define the performance baseline. The next chapter introduces detection theory, which provides the statistical framework for deciding whether a target is present based on the received signal.

Chapter 3

Detection Theory

In this chapter, we shift focus to the statistical framework used to determine target presence or absence amid random noise. Formulated as a binary hypothesis testing problem, we evaluate the null hypothesis H_0 (target absent, noise only) against the alternative hypothesis H_1 (target present). We define critical decision-making terminology: Type I errors represent false alarms (P_{FA} or significance level), while Type II errors signify missed targets, with the probability of detection (P_D) defining the statistical power of the test. Assuming an Additive White Gaussian Noise (AWGN) channel, we model each noise sample as an independent, identically distributed normal random variable with a flat power spectral density. In this environment, we apply the Neyman-Pearson criterion. This optimal approach allows us to design a decision rule that maximizes the probability of detection for a strictly fixed, user-defined probability of false alarm, entirely bypassing the need for prior target probabilities. We simplify this mathematical evaluation into a Likelihood Ratio Test (LRT). For known signals embedded in AWGN, we prove that this LRT reduces to a matched filter, which serves as the theoretically optimal classical detector by maximizing the output signal-to-noise ratio (SNR). We evaluate performance mathematically using the Gaussian Q-function to map the trade-off between P_{FA}, P_D, and SNR. Finally, we introduce Receiver Operating Characteristic (ROC) curves and the Area Under the Curve (AUC) metric as the standard tools to visualize detection capabilities under varying decision thresholds and SNR constraints.

- Introduction.
- What "Detection" Means Mathematically.
- Binary Hypothesis Testing Framework.
- Terminology (Type I/II errors, Power, Significance Level).
- Detection Performance Metrics ($\mathrm{P}_FA, P_D, SNR, Q - function$).
- Statistical Model for AWGN.
- The Neyman-Pearson Criterion.

- Likelihood Ratio Test and Matched Filter.
- Receiver Operating Characteristic (ROC) Curves.
- Interpreting ROC Curves and AUC.
- Conclusion.

3.1 Introduction

In this chapter, we formalize the optimal decision-theoretic framework necessary to ascertain target presence or absence within stochastic environments. Because the received radar return is inevitably corrupted by random fluctuations, we formulate the decision process as a binary hypothesis testing problem, evaluating the null hypothesis H_0 (target absent, noise-only observations) against the alternative hypothesis H_1 (target present, signal-plus-noise observations). We establish the fundamental statistical performance boundaries by defining Type I errors as the probability of false alarm (P_{FA} or significance level α) and Type II errors as the probability of a miss ($1 - P_{\text{D}}$), where the probability of detection (P_{D}) quantifies the statistical power of the test. Under the assumption of an Additive White Gaussian Noise (AWGN) channel characterized by a flat, double-sided power spectral density $N_0/2$, we model the observation vector via multivariate normal probability density functions $p(\mathbf{x}|H_0)$ and $p(\mathbf{x}|H_1)$. We then apply the Neyman-Pearson lemma to derive an optimal decision rule that maximizes P_{D} for a strictly constrained, user-defined upper bound on P_{FA}, entirely independent of prior hypothesis probabilities or cost assignments. We show that this constrained optimization simplifies into a Likelihood Ratio Test (LRT) of the form $\Lambda(\mathbf{x}) = \frac{p(\mathbf{x}|H_1)}{p(\mathbf{x}|H_0)} \gtrless_{H_0}^{H_1} \gamma$. For deterministic signals embedded in AWGN, we prove that this LRT simplifies to a linear operation, reducing the optimal receiver architecture to a matched filter that maximizes the output signal-to-noise ratio (SNR). Finally, we characterize the exact performance trade-offs using the Gaussian Q-function to analytically map P_{D}, P_{FA}, and SNR, subsequently utilizing Receiver Operating Characteristic (ROC) curves and the Area Under the Curve (AUC) metric as the definitive tools to evaluate detection performance under varying decision thresholds γ.

3.2 What "Detection" Means Mathematically

Detection is the process of deciding whether a target is present or absent based on noisy observations. This is formulated as a binary hypothesis testing problem, where the two hypotheses correspond to the target being absent (H_0) or present (H_1). The goal is to design a decision rule that optimally balances the probability of correct detection against the probability of false alarm.

3.2.1 Binary Hypothesis Testing Framework

$$\theta \in \Theta \quad \text{(the parameter space)}$$

Θ_0 and Θ_1 are subsets whose union equals Ω and intersection equals $\varnothing$.

$$H_0 : \theta \in \Theta_0$$

$$H_1 : \theta \in \Theta_1$$

Parametric Measurement Model:

$$p(x;\theta)$$

where x is the observation, θ is the parameter, and p is the probability density function (pdf). When viewed as a function of θ for a fixed observed x, $p(x;\theta)$ becomes the likelihood function, which helps determine the best θ to explain the observed x.

The Decision Rule:

$$\Phi(x) : \mathcal{X} \to \{0,1\}$$

$$\Phi(x) = \begin{cases} 1, & \text{decide } H_1 \\ 0, & \text{decide } H_0 \end{cases}$$

The data space $\mathcal{X}$ is partitioned:

$$\mathcal{X}_0 = \{x : \Phi(x) = 0\}, \quad \mathcal{X}_1 = \{x : \Phi(x) = 1\} \tag{3.1}$$

False Alarm:

$$P_{\text{fa}} = \mathbb{E}_{x|\theta}[\Phi(X)|\theta] = \int_{\mathcal{X}_1} p(x|\theta)\, dx, \quad \text{for } \theta \in \Theta_0 \tag{3.2}$$

Miss:

$$P_{\text{m}} = \mathbb{E}_{x|\theta}[1 - \Phi(X)|\theta] = 1 - \int_{\mathcal{X}_1} p(x|\theta)\, dx = \int_{\mathcal{X}_0} p(x|\theta)\, dx, \quad \text{for } \theta \in \Theta_1 \tag{3.3}$$

Probability of Detection:

$$P_{\text{d}} = 1 - P_{\text{m}} = \int_{\mathcal{X}_1} p(x|\theta)\, dx, \quad \text{for } \theta \in \Theta_1 \tag{3.4}$$

3.2.2 Terminology

- **Type I Error**: False Alarm
- **Type II Error**: Miss
- **Power**: Probability of Detection
- $P_{\mathbf{fa}}$: Significance Level

3.2.3 Detection Performance Metrics

While the formal definitions of false alarm and detection probabilities were introduced in Section 3.2, for the AWGN case with a matched filter detector, these quantities take explicit forms in terms of the Q-function.

Let the test statistic be $T(\mathbf{x}) = \sum_{n=0}^{N-1} x[n]s[n]$, and let the threshold be γ.

Under H_0, $T \sim \mathcal{N}(0, \sigma^2\mathcal{E})$.

Under H_1, $T \sim \mathcal{N}(\mathcal{E}, \sigma^2\mathcal{E})$, where $\mathcal{E} = \sum s[n]^2$ is the signal energy.

The false alarm and detection probabilities are:

$$P_{FA} = Q\left(\frac{\gamma}{\sqrt{\sigma^2\mathcal{E}}}\right), \tag{3.5}$$

$$P_D = Q\left(\frac{\gamma - \mathcal{E}}{\sqrt{\sigma^2\mathcal{E}}}\right), \tag{3.6}$$

where $Q(x) = \frac{1}{\sqrt{2\pi}} \int_x^\infty e^{-t^2/2} dt$ is the complementary cumulative distribution function of the standard normal distribution.

These expressions show that both metrics depend on:

- The threshold γ : chosen by the operator
- The noise variance σ^2 : determined by the receiver
- The signal energy $\mathcal{E}$: determined by transmit power and duration

For a fixed P_{FA}, the threshold is set as $\gamma = \sqrt{\sigma^2\mathcal{E}}\, Q^{-1}(P_{FA})$, and the resulting detection probability becomes:

$$P_D = Q\left(Q^{-1}(P_{FA}) - \sqrt{\text{SNR}}\right), \tag{3.7}$$

where $\text{SNR} = \mathcal{E}/\sigma^2$. This form is particularly useful for generating ROC curves, as it directly relates P_D to P_{FA} with SNR as a parameter.

3.2.3.1 Relation Between SNR and Test Statistic Variance

The signal-to-noise ratio is defined as $\text{SNR} = \mathcal{E}/\sigma^2$, where $\mathcal{E} = \sum s[n]^2$ is the signal energy and σ^2 is the noise variance.

Under hypothesis H_0, the test statistic $T = \sum x[n]s[n]$ has variance:

$$\text{Var}(T|H_0) = \sigma^2\mathcal{E}. \tag{3.8}$$

Using the definition of SNR, we can rewrite $\mathcal{E} = \sigma^2 \cdot \text{SNR}$. Substituting:

$$\sqrt{\text{Var}(T|H_0)} = \sqrt{\sigma^2 \cdot (\sigma^2 \cdot \text{SNR})} = \sigma^2\sqrt{\text{SNR}}. \tag{3.9}$$

Thus, the standard deviation of the test statistic scales with both the noise variance and the square root of SNR. This relation connects the physical quantities (signal energy, noise power) to the statistical quantities appearing in the Q-function expressions for P_{FA} and P_D.

In practice, this means that increasing SNR (by raising transmit power or integrating more pulses) directly increases the separation between the distributions under H_0 and H_1, making detection easier. Conversely, higher noise σ^2 increases the standard deviation, making the distributions overlap more and reducing detection performance.

3.3 Statistical Model for AWGN

3.3.1 White Noise Definition

A discrete-time random process $w[n]$ is said to be white if its samples are uncorrelated:

$$\mathbb{E}[w[i]w[j]] = \sigma^2\delta_{ij}, \tag{3.10}$$

where δ_{ij} is the Kronecker delta ($\delta_{ij} = 1$ if $i = j$, else 0). The power spectral density of white noise is flat across all frequencies:

$$P_{ww}(e^{j\omega}) = \sigma^2, \quad \omega \in [-\pi, \pi], \tag{3.11}$$

which explains the term "white" by analogy with white light containing all frequencies equally.

For a Gaussian white noise process, each sample is independently drawn from a normal distribution with zero mean and variance σ^2:

$$w[n] \sim \mathcal{N}(0, \sigma^2). \tag{3.12}$$

3.3.2 Probability Density Functions Under H_0 and H_1

Consider an observation vector $\mathbf{x} = (x[0], x[1], \ldots, x[N-1])^T$ consisting of N independent samples. Under the AWGN model, each sample is independently Gaussian with variance σ^2.

For a single Gaussian random variable x with mean μ and variance σ^2, the probability density function is:

$$p(x) = \frac{1}{\sqrt{2\pi\sigma^2}} \exp\left(-\frac{(x-\mu)^2}{2\sigma^2}\right). \tag{3.13}$$

For N independent samples, the joint PDF is the product of individual PDFs:

$$p(\mathbf{x}) = \prod_{n=0}^{N-1} \frac{1}{\sqrt{2\pi\sigma^2}} \exp\left(-\frac{(x[n]-\mu_n)^2}{2\sigma^2}\right). \tag{3.14}$$

The product of exponentials becomes the exponential of a sum, yielding:

$$p(\mathbf{x}) = \frac{1}{(2\pi\sigma^2)^{N/2}} \exp\left(-\frac{1}{2\sigma^2}\sum_{n=0}^{N-1}(x[n]-\mu_n)^2\right). \tag{1}$$

The structure of this PDF reflects three key facts:

- The **exponential form** produces the characteristic bell-shaped curve.
- The **quadratic deviation** $(x[n]-\mu_n)^2$ ensures symmetry: positive and negative errors are equally penalized.
- The **prefactor** $(2\pi\sigma^2)^{-N/2}$ guarantees that the total probability integrates to one.

For the binary hypothesis testing problem, the two hypotheses specify different mean vectors:

Hypothesis H_0 (Target absent): The observation consists of noise only, with zero mean:

$$x[n] = w[n], \quad \mathbb{E}[x[n]] = 0 \quad \forall n. \tag{3.15}$$

Substituting $\mu_n = 0$ into (1) gives:

$$\boxed{p(\mathbf{x}|H_0) = \frac{1}{(2\pi\sigma^2)^{N/2}} \exp\left(-\frac{1}{2\sigma^2}\sum_{n=0}^{N-1}x[n]^2\right)}. \tag{2}$$

Under this hypothesis, the probability depends only on the total energy of the observed samples. Observations with small sample values are more likely than those with large values.

Hypothesis H_1 (Target present): The observation contains a known deterministic signal $s[n]$ embedded in noise:

$$x[n] = s[n] + w[n], \quad \mathbb{E}[x[n]] = s[n]. \tag{3.16}$$

The mean becomes $\mu_n = s[n]$, and the deviation from the mean is exactly the noise: $x[n] - s[n] = w[n]$. Substituting into (1) yields:

$$\boxed{p(\mathbf{x}|H_1) = \frac{1}{(2\pi\sigma^2)^{N/2}} \exp\left(-\frac{1}{2\sigma^2}\sum_{n=0}^{N-1}(x[n]-s[n])^2\right)}. \tag{3}$$

Under this hypothesis, the probability is maximized when the observation closely matches the expected signal shape.

3.3.3 Connection to Detection

The likelihood ratio is formed by taking the ratio of (3) to (2):

$$\Lambda(\mathbf{x}) = \frac{p(\mathbf{x}|H_1)}{p(\mathbf{x}|H_0)} = \exp\left(-\frac{1}{2\sigma^2}\sum_{n=0}^{N-1}(x[n]-s[n])^2 + \frac{1}{2\sigma^2}\sum_{n=0}^{N-1}x[n]^2\right). \tag{3.17}$$

Expanding the first sum:

$$-\sum_{n=0}^{N-1}(x[n]^2 - 2x[n]s[n] + s[n]^2) + \sum_{n=0}^{N-1}x[n]^2 = 2\sum_{n=0}^{N-1}x[n]s[n] - \sum_{n=0}^{N-1}s[n]^2. \tag{3.18}$$

Thus:

$$\Lambda(\mathbf{x}) = \exp\left(\frac{1}{\sigma^2}\sum_{n=0}^{N-1}x[n]s[n] - \frac{1}{2\sigma^2}\mathcal{E}\right), \tag{3.19}$$

where $\mathcal{E} = \sum_{n=0}^{N-1} s[n]^2$ is the signal energy. Since the second term is constant for a known signal, the likelihood ratio test reduces to comparing the correlation $\sum x[n]s[n]$ against a threshold. This is the **matched filter**, the optimal detector for known signals in AWGN.

3.4 The Neyman-Pearson Criterion

The Neyman-Pearson criterion does not require prior probabilities or cost functions. Instead, it:

1. Fixes the false alarm probability $P_{FA} = \alpha$ (a desired level)
2. Maximizes the detection probability P_D subject to this constraint

The Neyman-Pearson lemma states that the most powerful test for a given P_{FA} is the likelihood ratio test [6]:

$$\Lambda(\mathbf{x}) = \frac{p(\mathbf{x}|H_1)}{p(\mathbf{x}|H_0)} \underset{H_0}{\overset{H_1}{\gtrless}} \gamma \tag{3.20}$$

where γ is chosen such that $P_{FA} = \alpha$.

3.5 Likelihood Ratio Test and Matched Filter

For the AWGN case with known signal $s[n]$:

$$p(\mathbf{x}|H_0) = \frac{1}{(2\pi\sigma^2)^{N/2}} \exp\left(-\frac{1}{2\sigma^2}\sum_{n=0}^{N-1} x[n]^2\right) \tag{3.21}$$

$$p(\mathbf{x}|H_1) = \frac{1}{(2\pi\sigma^2)^{N/2}} \exp\left(-\frac{1}{2\sigma^2}\sum_{n=0}^{N-1} (x[n]-s[n])^2\right) \tag{3.22}$$

The likelihood ratio becomes:

$$\Lambda(\mathbf{x}) = \exp\left(\frac{1}{\sigma^2}\sum_{n=0}^{N-1} x[n]s[n] - \frac{1}{2\sigma^2}\mathcal{E}\right) \tag{3.23}$$

where $\mathcal{E} = \sum s[n]^2$ is the signal energy. Since the second term is constant, the test reduces to comparing the correlation against a threshold:

$$T(\mathbf{x}) = \sum_{n=0}^{N-1} x[n]s[n] \underset{H_0}{\overset{H_1}{\gtrless}} \gamma' \tag{3.24}$$

This operation is called the **matched filter**. It computes how much the received signal resembles the transmitted signal. When the target is present, the correlation is large; when only noise is present, the correlation is small (randomly fluctuating around zero). The matched filter maximizes the output SNR for a known signal in white noise, making it the optimal linear [6].

3.6 The Deflection Coefficient: A General Detection Metric

The matched filter of the previous section is optimal for a *known* deterministic signal in additive Gaussian noise, and its performance is captured by a single quantity, $\sqrt{\text{SNR}}$, through $P_D = Q\big(Q^{-1}(P_{FA}) - \sqrt{\text{SNR}}\big)$. In general, however, a detector forms some decision statistic T whose value is compared against a threshold, and T need not be a matched filter on a known waveform. To analyse such detectors we use the *deflection coefficient*, a measure of how far apart the two hypotheses place the statistic T, expressed in units of its own spread.

3.6.1 Definition

Let T be the decision statistic, with means $\mu_0 = \mathbb{E}[T \mid H_0]$ and $\mu_1 = \mathbb{E}[T \mid H_1]$ and variances $\sigma_0^2 = \text{Var}(T \mid H_0)$ and $\sigma_1^2 = \text{Var}(T \mid H_1)$ under the two hypotheses. The (generalized)

deflection coefficient is [6]

$$d' = \frac{\mu_1 - \mu_0}{\sqrt{\frac{1}{2}\left(\sigma_0^2 + \sigma_1^2\right)}}. \tag{3.25}$$

The symmetrized denominator is used because, in the quantum problem treated later, the variance of the decision statistic differs under H_0 and H_1. When the two variances are equal, $\sigma_0 = \sigma_1 = \sigma$, this reduces to the familiar mean separation in noise standard deviations, $d' = (\mu_1 - \mu_0)/\sigma$.

3.6.2 The deflection coefficient governs the ROC

Assume the decision statistic is approximately Gaussian under both hypotheses (justified below by mode averaging). Deciding H_1 when $T > \gamma$, the false-alarm and detection probabilities are, by definition,

$$P_{FA} = Q\Big(\frac{\gamma - \mu_0}{\sigma}\Big), \qquad P_D = Q\Big(\frac{\gamma - \mu_1}{\sigma}\Big). \tag{3.26}$$

Eliminating the threshold γ from the first expression gives $\gamma = \mu_0 + \sigma\, Q^{-1}(P_{FA})$, and substituting into the second yields

$$P_D = Q\Big(Q^{-1}(P_{FA}) - \frac{\mu_1 - \mu_0}{\sigma}\Big) = Q\Big(Q^{-1}(P_{FA}) - d'\Big). \tag{3.27}$$

Equation (3.27) shows that the entire ROC curve is controlled by the single number d'. The threshold γ only moves the operating point *along* a fixed curve, whereas d' sets the *shape* of the curve itself: $d' = 0$ gives $P_D = P_{FA}$ (the random-guessing diagonal), and increasing d' bows the curve toward the ideal top-left corner. The deflection coefficient is therefore the primary figure of merit through which we compare detectors, and it generalizes the $\sqrt{\mathrm{SNR}}$ of the matched filter, which is simply Eq. (3.25) evaluated for a known signal in white noise.

3.6.3 Classical and quantum evaluations

The definition (3.25) is one expression evaluated for different detectors. For the optimal classical coherent-state receiver against a thermal background, the per-mode deflection is [10, 15]

$$D^2 = \frac{4\,\eta\, N_S}{2N_B + 1}, \tag{3.28}$$

where η is the round-trip transmissivity, N_S the mean signal photons per mode, and N_B the background photons per mode; in the lossless limit $\eta \to 1$ this is the textbook $4N_S/(2N_B{+}1)$. For the quantum correlation receiver $C = X_s X_i - P_s P_i$ used in Chapter 6, the means and variances in Eq. (3.25) are obtained from $\langle C \rangle$ and $\mathrm{Var}(C)$ computed from the post-channel covariance matrix; the resulting deflection is evaluated numerically there. The quantum advantage is precisely the ratio of these two deflections.

3.6.4 Multimode scaling

When M independent, identically prepared mode pairs are integrated, the summed decision statistic has mean proportional to M and variance proportional to M, so the deflection

grows as

$$d'(M) = \sqrt{M}\, d'_1, \tag{3.29}$$

where d'_1 is the single-mode value. The Gaussian approximation underlying Eq. (3.27) is justified, in this regime, by the central limit theorem applied to the sum over the $M = B\tau$ modes (the time–bandwidth product); the same averaging is what produces the $\sqrt{M}$ scaling.

3.7 Receiver Operating Characteristic (ROC) Curves

The Receiver Operating Characteristic (ROC) curve is the fundamental tool for visualizing detection performance. It plots the probability of detection P_D against the probability of false alarm P_{FA} as the decision threshold γ varies.

3.7.1 Interpreting ROC Curves

The ROC curve is read as follows:

- The **diagonal line** ($P_D = P_{FA}$) represents random guessing, a useless detector.
- A curve **above the diagonal** indicates better-than-random performance.
- The **further the curve is from the diagonal** (closer to the top-left corner), the better the detector.
- The **Area Under the Curve (AUC)** is a single-number summary: AUC = 1 is perfect detection, AUC = 0.5 is random guessing.

For radar applications, typical operating points aim for $P_{FA} = 10^{-6}$ (one false alarm per million scans) and $P_D \geq 0.9$.

Each point on a ROC curve corresponds to a different threshold:

- A **low threshold** yields both high P_D and high P_{FA} : many detections but also many false alarms.
- A **high threshold** yields both low P_D and low P_{FA} : few false alarms but also missed targets.

The Neyman-Pearson criterion selects the operating point on this curve that fixes P_{FA} at a desired level while maximizing P_D. As SNR increases, the ROC curve shifts toward the top-left corner, indicating better detection performance.

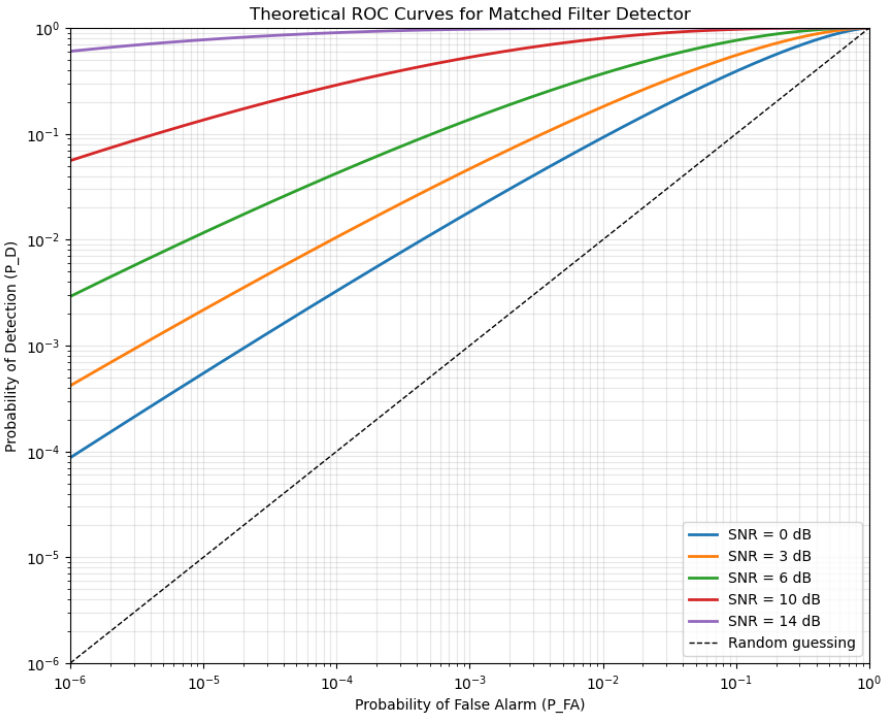

Figure 3.1: Theoretical ROC curves for a matched filter detector in AWGN at different SNR values.

Figure 3.1 shows theoretical ROC curves for SNR values of 0, 3, 6, 10, and 14 dB. The curve approaches the top-left corner as SNR increases. The dashed diagonal line represents random guessing ($P_D = P_{FA}$), which any useful detector must exceed.

3.8 Conclusion

In this chapter, we established the statistical and decision-theoretic foundations of detection theory, providing the rigorous mathematical baseline necessary to benchmark classical system performance against non-classical radar architectures. We formalized the problem of target identification within an Additive White Gaussian Noise (AWGN) channel as a binary hypothesis testing problem, evaluating the null hypothesis H_0 of noise-only observations against the alternative hypothesis H_1 representing signal-plus-noise observations. We mapped the exact boundaries of operational error and statistical power by defining Type I errors as false alarms (P_{FA} or significance level) and Type II errors as missed targets, where the probability of detection (P_{D}) quantifies the performance capability of our decision rule. By applying the Neyman-Pearson criterion, we've shown that the optimal radar decision rule maximizes P_{D} for a strictly fixed, user-defined constraint on P_{FA} without requiring prior target probabilities. We demonstrated that this constrained optimization evaluates down to a Likelihood Ratio Test (LRT), which for known deterministic signals embedded in independent Gaussian samples mathematically simplifies to a linear matched filter receiver that maximizes the output signal-to-noise ratio (SNR). We analytically characterized performance using the Gaussian Q-function to relate decision thresholds to P_{FA} and P_{D}, showing that standard deviations and distribution separation scale fundamentally with $\sqrt{\text{SNR}}$. Finally, we introduced Receiver Operating Characteristic (ROC) curves and the Area Under

the Curve (AUC) metric as the definitive tools to visualize and summarize classical detector performance as decision thresholds shift. Together, these statistical principles bound the performance capabilities of classical radar systems, completing the analytical baseline needed to quantify quantum enhancement in subsequent chapters.

Chapter 4

Discovering Quantum Radars

This Chapter builds the core theoretical, mathematical, and conceptual physics framework underpinning the Quantum Illumination (QI) protocol. It explains how non-linear crystal architectures are used to generate Two-Mode Squeezed Vacuum (TMSV) states consisting of highly entangled signal and idler photon pairs. Although the physical entanglement between the transmitted signal and retained idler is completely destroyed by catastrophic environmental losses and intense thermal noise, the protocol succeeds by exploiting the non-classical "quantum tag" history of correlations via a joint measurement receiver. By applying Continuous Variable (CV) phase space mathematics to characterize zero-mean Gaussian states through Covariance Matrices (V), the chapter uses the Quantum Chernoff Bound (QCB) to derive a fundamental 4-factor (6 dB) error probability exponent advantage for an idealized quantum joint receiver over an energy-matched classical coherent radar, noting that physically implementable structured receivers recover half of this ceiling to achieve an approximate 3 dB advantage.

- Introduction.
- The Quantum Illumination Protocol.
- Core Mathematical Framework.
- What Does a Quantum State Actually Describe?
- Superposition, Joint Quantum States, and Density Matrices.
- What Phase Means Here: A Relational and Intu- itive View.
- Principles of Classical and Quantum Radar as Hypothesis Testing.
- Resource Generation: Two-Mode Squeezed Vac- uum (TMSV).
- Gaussian States, Quadratures, and Covariance Matrices.
- Operator-Level Derivation of Noise and Correlation Parameters.
- Quantum Chernoff Bound and the Emergence of the 6 dB Advantage.

- Conclusion.

4.1 Introduction: Why Quantum Radar?

Classical radar systems are built on a simple and powerful idea: transmit a known electromagnetic signal, wait for a reflection, and correlate the received waveform with a stored reference. When the reflected signal is sufficiently strong compared to the background noise, this method works remarkably well. In fact, most modern radar and sensing systems are sophisticated implementations of this basic principle.

However, this approach encounters fundamental limitations in regimes where the reflected signal is extremely weak. This situation arises naturally in long-range detection, low-reflectivity targets, stealth technology, or environments dominated by thermal noise. In such cases, the received signal becomes almost indistinguishable from noise, and classical correlation techniques approach their optimal performance limits.

A natural classical response is to increase the transmitted power. Yet, power is not always a free resource. Regulatory constraints, power budgets, detectability concerns, and physical limitations all impose bounds on how much energy can be transmitted. More importantly, even when power can be increased, classical detection strategies still face a noise-dominated regime in which performance improves only marginally.

Quantum radar, and more specifically *quantum illumination*, proposes a fundamentally different approach. Instead of increasing energy, it aims to increase *structure*. The idea is not to send a stronger signal, but to send a signal that is more informative at a statistical level, by exploiting quantum correlations.

What makes this proposal counterintuitive — and therefore interesting — is that quantum illumination claims an advantage precisely in regimes where quantum effects are usually thought to be fragile. The environment is assumed to be noisy, lossy, and decohering. Entanglement between transmitted and retained modes is largely destroyed. And yet, a detection advantage remains.

This raises the central question that motivates this chapter:

> *How can quantum correlations improve detection performance when the environment seems to erase all quantum features?*

Answering this question requires rethinking what information a quantum state actually carries, how detection is formulated as a hypothesis testing problem, and what role correlations play beyond classical signal processing intuition.

4.2 The Quantum Illumination Protocol

The Quantum Illumination (QI) protocol is a sensing paradigm designed to detect targets in environments where signal loss is high and background noise is intense.

4.2.1 Conceptual Step-by-Step of the QI Protocol

1. **Generation of Entanglement (TMSV States):** The protocol begins at the transmitter with a source; typically a non-linear crystal using Spontaneous Parametric Down-Conversion (SPDC) or a Josephson Parametric Amplifier (JPA). This source generates a Two-Mode Squeezed Vacuum (TMSV) state, a non-classical Gaussian state consisting of two highly correlated modes: the **signal** and the **idler**.

2. **Roles of the Modes:** The **signal mode** is transmitted toward a region of space where a target may be located. The **idler mode** is retained locally at the receiver to serve as a high-fidelity reference.

3. **The Lossy/Noisy Channel:** In a realistic radar scenario, the signal encounters a weakly-reflecting target ($\kappa \ll 1$) embedded in a bright thermal background ($N_B \gg 1$). As the signal travels to the target and back, the combination of extreme loss and thermal noise destroys the original entanglement between the signal and idler.

4. **Retention of the Idler (Quantum Memory):** While the signal mode travels, the idler must be stored locally. This requires a quantum memory or a delay line to ensure the idler is available for recombination at the exact moment the reflected signal (the echo) returns.

5. **Joint vs. Classical Measurement:** In a classical radar, the receiver independently measures the returning echo's properties. In QI, the receiver performs an **optimal joint measurement** (a simultaneous measurement on both the returning signal and the stored idler). This joint measurement extracts the residual non-classical correlations that persist between the modes, even after their entanglement has been broken.

6. **Performance in Entanglement-Breaking Channels:** QI is uniquely robust because it does not require entanglement to *exist* at the detector. Instead, it exploits the *history of entanglement*; the measurement identifies whether the received photons *could have been* entangled with the idler, allowing the receiver to distinguish signal echoes from background noise with a precision that exceeds any classical system.

4.2.2 Conceptual Diagram of the QI Protocol

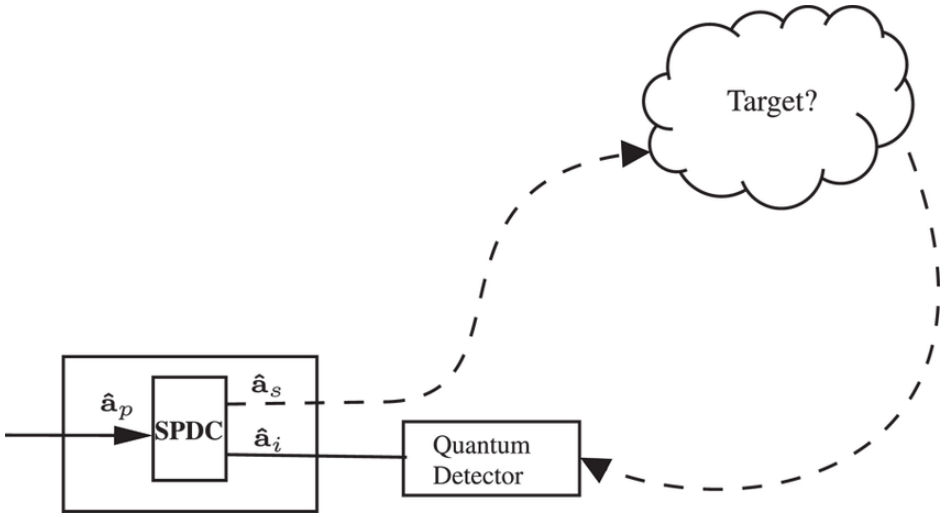

Figure 4.1: Conceptual diagram of the Quantum Illumination protocol, showing the entangled source, signal transmission through the lossy thermal-noise channel, idler retention, and joint measurement for target detection. Adapted from [4].

4.2.3 Key Parameters Defined

Parameter	Definition
κ	Transmissivity / reflectivity: fraction of signal power returning after reflecting off the target ($\kappa \ll 1$ in QI regime).
N_S	Signal photon number: mean signal photons per mode ($N_S \ll 1$ in QI regime).
N_B	Noise photon number: mean background thermal noise photons per mode ($N_B \gg 1$ in QI regime).
r	Squeezing parameter: quantifies the degree of non-classical correlation (higher r = stronger entanglement).
M	Number of modes: total signal-idler pairs integrated per detection event ($M = B\tau$, the time-bandwidth product).

Table 4.1: Key parameters in quantum illumination and their typical regimes for the quantum advantage.

4.2.4 The Counterintuitive Nature of QI

Quantum Illumination is fundamentally counterintuitive because it leverages a fragile resource **entanglement** to improve performance in environments specifically designed to destroy that resource. In most quantum technologies, such as quantum computing, the loss of entanglement (decoherence) is catastrophic. However, QI operates as an **entanglement-breaking** protocol; it accepts the inevitable destruction of entanglement by noise and loss, yet still yields a detection advantage.

This works because the initial entanglement imprints a unique **non-classical coherence** on the modes that cannot be entirely erased by thermal noise, effectively providing a "quantum tag" on the signal photons that makes them distinguishable from identical-looking noise photons.

4.3 Core Mathematical Framework

4.3.1 Quantum States and Hilbert Spaces

Quantum mechanics describes an isolated physical system using a **state vector** $|\psi\rangle$, which is a unit vector in a complex vector space known as a **Hilbert space**. When a system's state is not known exactly, it is described by a **density operator** ρ [8], defined as a positive semidefinite operator with unit trace:

$$\rho \geq 0, \quad \mathrm{Tr}(\rho) = 1.$$

The expected value of any observable F is given by the trace formula:

$$\mathbb{E}(F) = \mathrm{Tr}(\rho F). \tag{4.1}$$

This replaces the classical probability density function in quantum statistical theory.

4.3.2 Unitary Evolution and Hamiltonians

The time evolution of a closed quantum system is governed by **Schrödinger's equation**, producing a **unitary transformation** U applied to the state. The **Hamiltonian** H represents the total energy of the system and acts as the generator of these unitary transformations.

4.3.3 Composite Systems and Tensor Products

When multiple systems (such as a radar's signal and reference idler) are combined, their joint state space is the **tensor product** of their individual Hilbert spaces. For subsystems S and I:

$$\mathcal{H}_{SI} = \mathcal{H}_S \otimes \mathcal{H}_I. \tag{4.2}$$

A general joint state takes the form

$$|\psi_{SI}\rangle = \sum_{m,n} c_{mn} |m\rangle_S \otimes |n\rangle_I. \tag{4.3}$$

States that cannot be factorized as $|\alpha\rangle_S \otimes |\beta\rangle_I$ are called *entangled*. Entanglement is not merely a strong correlation; it is a structural property of the joint state with no classical analogue.

4.4 What Does a Quantum State Actually Describe?

Before discussing quantum radar, it is essential to clarify what a quantum state represents. A photon's degrees of freedom may include polarization, frequency (or spectral mode), spatial mode, time of arrival, and phase. Importantly, these properties are not all equivalent in nature.

This distinction hints at a deeper idea: quantum states are not merely descriptions of isolated systems, but of *relations*. Many physically meaningful quantities emerge only when systems are considered together, either through interference, comparison, or joint measurement.

Furthermore, quantum states are inherently statistical objects. Even when a system is prepared in a well-defined state, repeated measurements yield probabilistic outcomes. The state does not predict a single event, but an ensemble of outcomes and their correlations.

4.4.1 What Phase Means Here: A Relational and Intuitive View

At first, the notion of *phase* is confusing in the context of quantum illumination. In classical signal processing, phase is often understood as a temporal shift: a waveform arrives earlier or later in time. With this intuition, it is natural to ask: *what does phase even mean for a photon, or for a quantum state, especially in a noisy environment where everything seems randomized?*

The key realization is that, in quantum mechanics, phase is not an absolute property of an individual system. Phase is fundamentally *relational*. It only acquires meaning when two or more modes are compared, interfered, or statistically related.

4.4.1.1 Phase Is Not a Time Shift

In the Gaussian-state description used in quantum illumination, phase does not appear as a delay parameter. Instead, it is encoded in the relative orientation of quadratures in phase space. Mathematically, this shows up through sign structures such as the matrix

$$Z = \mathrm{diag}(1, -1),$$

which distinguishes correlations between position-like and momentum-like quadratures.

A single noisy mode, taken alone, does not carry usable phase information. Just like a single number has no direction without a reference frame, a single quantum mode has no meaningful phase without another mode to compare it to.

4.4.1.2 A Social Analogy for Quantum Phase and Coherence

An intuitive way to understand this is to think of a quantum system as a society:

- The *modes* of the quantum system are like *individuals* in a society.

- The *phase relations* between modes are like how much people align with each other.
- A *coherent* quantum state corresponds to a society where relationships are structured and aligned.
- An *incoherent* or thermal state corresponds to a society where interactions are random and uncorrelated.

In this picture, the quantum state is not defined by any single individual, but by the *pattern of relationships* across the whole society. Noise does not necessarily destroy all structure; even if individuals behave randomly, faint but non-random patterns of interaction may still exist. These patterns are what we refer to as *residual correlations*.

4.4.1.3 Measurement as an Outsider's Inference

Quantum hypothesis testing can then be understood as an outsider entering this society and trying to infer the global structure from statistical evidence alone. In quantum illumination, the Helstrom measurement plays the role of this outsider. It does not identify individual photons or trajectories. Instead, it infers which global state is more likely based on subtle statistical differences in correlations.

4.4.1.4 Why This Matters for Detection

If phase were merely a time shift, strong thermal noise would erase it completely. However, because phase lives inside *joint statistics* rather than individual signals, it can survive in a statistical sense. Classical radar mostly accesses individual-mode information. Quantum illumination accesses *relational* information. This difference explains why a detection advantage remains even in extremely noisy environments.

4.5 Superposition, Joint Quantum States, and Density Matrices

4.5.1 Superposition in Single Systems

One of the defining features of quantum mechanics is superposition. A quantum system can exist in a linear combination of basis states:

$$|\psi\rangle = \sum_n c_n |n\rangle, \tag{4.4}$$

where the complex coefficients c_n encode both amplitudes and relative phases. The presence of complex amplitudes means that probabilities are not added directly; instead, amplitudes *interfere*. This interference is responsible for many non-classical effects.

4.5.2 Density Matrix Formalism

In realistic scenarios, systems interact with environments, experience loss, and undergo decoherence. As a result, pure-state descriptions are often insufficient. The appropriate formalism is that of **density matrices**.

For a pure state:

$$\rho = |\psi\rangle\langle\psi|. \tag{4.5}$$

For a mixed state:

$$\rho = \sum_k p_k |\psi_k\rangle\langle\psi_k|, \tag{4.6}$$

where p_k are classical probabilities. The diagonal elements represent populations, while the off-diagonal elements represent *coherence*; interference between states.

4.5.3 Interference, Coherence, and Off-Diagonal Terms

The physical meaning of off-diagonal terms is central to quantum illumination. When a system interacts with a noisy environment, these off-diagonal terms are often suppressed, a process known as *decoherence*.

However, suppression does not necessarily mean complete elimination. Even when coherence is strongly reduced, small residual off-diagonal terms may remain. These residual structures are not directly observable in single-mode measurements, but they *can* influence joint statistics. This is a key precursor to the quantum illumination advantage: even when entanglement is largely destroyed, remnants of the original joint structure persist statistically.

4.5.4 Separability and Entanglement

A state is **separable** if it can be written as a convex mixture of product states:

$$\rho = \sum_k p_k \, \rho_S^{(k)} \otimes \rho_I^{(k)}, \tag{4.7}$$

representing only classical correlations. A state that cannot be written this way is **entangled**. In a radar environment, entanglement is typically broken by noise and loss as the signal travels to the target. However, quantum illumination exploits the *residual* non-classical correlations that remain even after entanglement is lost.

4.6 Principles of Classical and Quantum Radar as Hypothesis Testing

At its core, radar detection is not about observing a signal directly, but about making a decision under uncertainty. The physical question "is there a target?" is translated into a statistical hypothesis testing problem:

$$\begin{cases} H_0 : \text{Target absent} \\ H_1 : \text{Target present} \end{cases}$$

4.6.1 Measurements: POVMs

Quantum measurements are described by a **Positive Operator-Valued Measure (POVM)** [8, 20], a set of operators $\{M_k\}$ satisfying $\sum_k M_k^\dagger M_k = \mathbb{I}$. The probability of outcome k given state ρ is $p(k) = \mathrm{Tr}(M_k^\dagger M_k \rho)$.

4.6.2 Joint vs. Independent Measurement

A **joint measurement** is a simultaneous measurement performed on both the returned signal and the retained idler. It is required to achieve the full 6 dB quantum advantage in standard quantum illumination, but it requires a **quantum memory** to store the idler. In **Quantum Two-Mode Squeezing (QTMS)** radar [21], the signal and idler are measured independently (typically using I/Q demodulators), removing the need for quantum memory but generally yielding a smaller (3 dB) advantage.

4.6.3 Classical Radar Formulation

In a classical radar, the transmitted signal is a known coherent waveform with average photon number N_S. The received field is modeled as the sum of a reflected signal (if the target is present) and thermal noise with mean photon number N_B.

Under H_0, the received mode contains only thermal noise:

$$\rho_0^{(C)} = \rho_{\mathrm{th}}(N_B). \tag{4.8}$$

Under H_1, the received mode contains a weak reflected signal with reflectivity $\kappa \ll 1$:

$$\rho_1^{(C)} = \rho_{\mathrm{th}}(N_B + \kappa N_S). \tag{4.9}$$

The optimal classical receiver performs a measurement that minimizes the probability of error. In the asymptotic limit of many independent uses (M modes), the minimum achievable error probability decays exponentially:

$$P_e^{(C)} \sim e^{-M\xi_C}. \tag{4.10}$$

In the noise-dominated regime ($N_B \gg 1$, $N_S \ll 1$, $\kappa \ll 1$), the classical error exponent scales as [10]:

$$\xi_C \approx \frac{\kappa N_S}{4N_B}. \tag{4.11}$$

The **ROC curve** relates the Probability of Detection (P_d) to the Probability of False Alarm (P_{fa}) for Gaussian states:

$$P_d = \mathrm{erfc}\Big[\mathrm{erfc}^{-1}(P_{fa}) - \sqrt{M}\, D\Big], \tag{4.12}$$

where D is the equivalent SNR, with $D^2 = \frac{4N_S}{2N_B+1}$ for detection in thermal radiation.

4.6.4 Quantum Radar (Quantum Illumination) Formulation

Quantum illumination modifies the detection problem by introducing a joint quantum state between two modes:

- **Signal mode** (S): transmitted toward the target.
- **Idler mode** (I): retained at the receiver.

Initially, these two modes are prepared in an entangled state, typically a **Two-Mode Squeezed Vacuum (TMSV)** state:

$$|\psi_{SI}\rangle = \sum_{n=0}^{\infty} \sqrt{\frac{N_S^n}{(N_S+1)^{n+1}}} |n\rangle_S |n\rangle_I. \tag{4.13}$$

The signal mode interacts with the environment and possibly reflects off a target, while the idler mode remains isolated. Detection is performed *jointly* on the returned mode R and the idler I.

Under H_0:

$$\rho_0 = \rho_{\text{th}}(N_B) \otimes \rho_I \quad \text{(no correlation between } R \text{ and } I\text{)}. \tag{4.14}$$

Under H_1:

$$\rho_1 = \rho_{RI} \quad \text{(residual correlations from initial entanglement)}. \tag{4.15}$$

The key point is that the difference between H_0 and H_1 is not primarily in the marginal statistics of R, but in the *joint statistics* of (R, I).

4.7 Resource Generation: Two-Mode Squeezed Vacuum (TMSV)

The TMSV is a fundamental **Gaussian state** used in quantum illumination. It is generated via processes like **spontaneous parametric down-conversion (SPDC)** in a nonlinear crystal, or a **Josephson Parametric Amplifier (JPA)**.

TMSV states have zero mean field and a covariance matrix where off-diagonal elements represent quantum correlations that exceed what is classically possible. The term *squeezing* refers to the redistribution of quantum noise between the in-phase (I) and quadrature (Q) components; while the product of uncertainties remains bounded by the Heisenberg uncertainty principle, the noise in one quadrature is reduced at the expense of the other.

The standard Beam Splitter Hamiltonian governing the interaction of two modes (a, b) is:

$$H_{\text{bs}} = i\theta\Big(ab^\dagger - a^\dagger b\Big), \tag{4.16}$$

resulting in the unitary transformation $B = \exp[\theta(a^\dagger b - ab^\dagger)]$.

4.8 Gaussian States, Quadratures, and Covariance Matrices

4.8.1 Quadrature Representation

Conventions used throughout this thesis.

Unless stated otherwise, we adopt the unscaled quadrature convention:

- Quadratures: $\hat{x} = \hat{a} + \hat{a}^\dagger, \quad \hat{p} = i(\hat{a}^\dagger - \hat{a})$.
- Commutator: $[\hat{x}, \hat{p}] = 2i$.
- Vacuum variance: $\langle \hat{x}^2 \rangle_{\text{vac}} = \langle \hat{p}^2 \rangle_{\text{vac}} = 1$.
- Covariance matrix: $V_{jk} = \frac{1}{2}\langle \{\hat{R}_j - \langle \hat{R}_j \rangle,\ \hat{R}_k - \langle \hat{R}_k \rangle\} \rangle$, with $\hat{R} = (\hat{x}_s, \hat{p}_s, \hat{x}_i, \hat{p}_i)^\top$.
- Vacuum covariance $V_{\text{vac}} = \mathbb{I}$; thermal covariance $V_{\text{th}} = (2\bar{n} + 1)\mathbb{I}$.
- Uncertainty relation: $V + i\Omega \geq 0$, with $[\hat{R}_j, \hat{R}_k] = 2i\,\Omega_{jk}$.
- Mean photon numbers: $N_S = \sinh^2 r$ (signal brightness), N_B (background per mode), η (round-trip transmissivity).

In continuous-variable quantum optics, bosonic modes are described using quadrature operators:

$$\hat{x} = \hat{a} + \hat{a}^\dagger, \qquad \hat{p} = i(\hat{a}^\dagger - \hat{a}). \tag{4.17}$$

For a two-mode system (returned mode R and idler I), we define the quadrature vector:

$$\hat{\mathbf{X}} = (\hat{x}_R, \hat{p}_R, \hat{x}_I, \hat{p}_I)^T. \tag{4.18}$$

A Gaussian quantum state is fully characterized by its mean vector (here zero) and its covariance matrix V with elements:

$$V_{jk} = \frac{1}{2}\langle \hat{X}_j \hat{X}_k + \hat{X}_k \hat{X}_j \rangle. \tag{4.19}$$

4.8.2 Covariance Matrices Under Each Hypothesis

In quantum illumination, both hypotheses correspond to zero-mean Gaussian states, differing only in their covariance structure.

Hypothesis H_0 (No target): The returned mode is thermal and uncorrelated with the idler:

$$V_0 = \begin{pmatrix} a_0 I_2 & 0 \\ 0 & a I_2 \end{pmatrix}, \tag{4.20}$$

where $a_0 = 2N_B + 1$ and $a = 2N_S + 1$.

Hypothesis H_1 (Target present): The returned mode is weakly correlated with the idler:

$$V_1 = \begin{pmatrix} a_R I_2 & C_R Z \\ C_R Z & a I_2 \end{pmatrix}, \tag{4.21}$$

with

$$a_R = 2(\kappa N_S + N_B) + 1, \qquad C_R = 2\sqrt{\kappa N_S(N_S+1)}, \qquad Z = \mathrm{diag}(1,-1). \tag{4.22}$$

Physical meaning:

- a_0, a_R: noise-dominated variances of the returned mode.
- a: idler variance.
- C_R: residual correlation originating from the initial entanglement.

The initial TMSV state itself has covariance matrix:

$$V_{\mathrm{TMSV}} = \begin{pmatrix} (2N_S+1)\, I_2 & 2\sqrt{N_S(N_S+1)}\, Z \\ 2\sqrt{N_S(N_S+1)}\, Z & (2N_S+1)\, I_2 \end{pmatrix}, \tag{4.23}$$

where $N_S = \sinh^2 r$ and r is the squeezing parameter.

4.8.3 Continuous Variables and Phase Space

Quantum continuous variables (CV) provide the mathematical framework for systems with infinite-dimensional degrees of freedom, such as quantum harmonic oscillators and optical modes. This formalism is central to quantum optics and quantum illumination.

4.8.3.1 Quadrature Operators

Instead of working directly with creation and annihilation operators $\hat{a}, \hat{a}^\dagger$, the CV formalism groups the canonical position and momentum of each mode into a vector:

$$\hat{\mathbf{r}} = (\hat{x}_1, \hat{p}_1, \ldots, \hat{x}_n, \hat{p}_n)^\top, \tag{4.24}$$

where $\hat{x} = \hat{a} + \hat{a}^\dagger$ and $\hat{p} = i(\hat{a}^\dagger - \hat{a})$. These operators obey the canonical commutation relations:

$$[\hat{r}_i, \hat{r}_j] = 2i\,\Omega_{ij}, \tag{4.25}$$

where Ω is the symplectic form.

4.8.3.2 Gaussian States

A state is **Gaussian** if its Wigner function in phase space is a multivariate Gaussian [22]. It is fully characterized by:

- The **first moment** (displacement vector): $\mathbf{d} = \langle \hat{\mathbf{r}} \rangle$
- The **second moment** (covariance matrix): $V_{ij} = \frac{1}{2}\langle \{\hat{r}_i - d_i, \hat{r}_j - d_j\} \rangle$

To satisfy the Heisenberg uncertainty principle, the covariance matrix must satisfy:

$$V + i\Omega \geq 0. \tag{4.26}$$

4.8.3.3 Gaussian Operations

Gaussian unitaries map Gaussian states to Gaussian states. In phase space, they correspond to symplectic transformations:

$$\hat{\mathbf{r}} \to S\hat{\mathbf{r}}, \qquad V \to SVS^{\top},$$

where S is a symplectic matrix ($\det S = 1$). Common Gaussian operations include beam splitters, phase shifters, and squeezing transformations.

4.8.3.4 Why the Gaussian Formalism Is Powerful

Because Gaussian states are fully defined by their first and second moments, they drastically reduce complexity. An infinite-dimensional Hilbert space is reduced to a finite set of parameters (a displacement vector and a covariance matrix). This allows analytical evaluation of entropy, entanglement (via the Peres-Horodecki criterion), and transmission through Gaussian channels, all essential for quantum illumination.

4.9 Operator-Level Derivation of Noise and Correlation Parameters

4.9.1 Two-Mode Squeezing Transformation

A TMSV state is generated by the unitary:

$$\hat{U}(r) = \exp\left[r\left(\hat{a}_S\hat{a}_I - \hat{a}_S^{\dagger}\hat{a}_I^{\dagger}\right)\right]. \tag{4.27}$$

The annihilation operator of the signal mode transforms as:

$$\hat{a}'_S = \hat{U}^{\dagger}\hat{a}_S\hat{U} = \hat{a}_S\cosh r + \hat{a}_I^{\dagger}\sinh r, \tag{4.28}$$

and correspondingly:

$$\hat{a}_S'^{\dagger} = \hat{a}_S^{\dagger}\cosh r + \hat{a}_I\sinh r. \tag{4.29}$$

4.9.2 Quadrature Operators and Variances

The signal quadratures are:

$$\hat{x}_S = \hat{a}'_S + \hat{a}'^{\dagger}_S, \qquad \hat{p}_S = i(\hat{a}'^{\dagger}_S - \hat{a}'_S). \tag{4.30}$$

Their variances are computed via vacuum expectation values $\langle\cdot\rangle = \langle 0_S 0_I| \cdot |0_S 0_I\rangle$:

$$\langle \hat{x}_S^2 \rangle = \langle (\hat{a}'_S + \hat{a}'^{\dagger}_S)^2 \rangle = \langle \hat{a}'_S \hat{a}'^{\dagger}_S \rangle + \langle \hat{a}'^{\dagger}_S \hat{a}'_S \rangle. \tag{4.31}$$

Using the canonical relations $\langle \hat{a}\hat{a}^\dagger \rangle = 1$, $\langle \hat{a}\hat{a} \rangle = 0$, $\langle \hat{a}^\dagger \hat{a}^\dagger \rangle = 0$, one finds:

$$\langle \hat{a}'_S \hat{a}'^{\dagger}_S \rangle = \cosh^2 r \, \langle \hat{a}_S \hat{a}^\dagger_S \rangle + \sinh^2 r \, \langle \hat{a}^\dagger_I \hat{a}_I \rangle + \ldots = \cosh^2 r. \tag{4.32}$$

$$\langle \hat{a}'^{\dagger}_S \hat{a}'_S \rangle = \sinh^2 r. \tag{4.33}$$

Therefore:

$$\langle \hat{x}_S^2 \rangle = \langle \hat{p}_S^2 \rangle = \cosh^2 r + \sinh^2 r = \cosh(2r). \tag{4.34}$$

4.9.3 Connection to Mean Photon Number

The mean photon number of the signal mode is:

$$N_S = \sinh^2 r. \tag{4.35}$$

Using $\cosh(2r) = 2\sinh^2 r + 1$, the quadrature variances become:

$$\boxed{\langle \hat{x}_S^2 \rangle = \langle \hat{p}_S^2 \rangle = 2N_S + 1.} \tag{4.36}$$

This quantity defines the signal variance parameter $a = 2N_S + 1$ in the covariance matrix.

4.9.4 Beam-Splitter Channel at the Operator Level

The lossy channel is modeled as a beam splitter of transmissivity η [23] mixing the signal mode $\hat{a}$ with a thermal environment mode $\hat{b}$:

$$\hat{a}' = \sqrt{\eta}\,\hat{a} + \sqrt{1-\eta}\,\hat{b}, \qquad \hat{b}' = -\sqrt{1-\eta}\,\hat{a} + \sqrt{\eta}\,\hat{b}. \tag{4.37}$$

The unitary generator is:

$$U_{\mathrm{BS}}(\theta) = \exp\left[\theta\left(\hat{a}\hat{b}^\dagger - \hat{a}^\dagger \hat{b}\right)\right], \qquad \cos^2\theta = \eta. \tag{4.38}$$

The output state is:

$$\rho_{\mathrm{out}} = \mathrm{Tr}_{\mathrm{env}}\left[U_{\mathrm{BS}}\left(\rho_{\mathrm{signal}} \otimes \rho_{\mathrm{env}}\right) U_{\mathrm{BS}}^\dagger\right]. \tag{4.39}$$

At the level of covariance matrices, this becomes:

$$V_{\mathrm{out}} = \eta\, V_{\mathrm{in}} + (1-\eta)(2N_B + 1)\, I. \tag{4.40}$$

4.10 Quantum Chernoff Bound and the Emergence of the 6 dB Advantage

4.10.1 Quantum Chernoff Bound

For two quantum states ρ_0 and ρ_1, the optimal asymptotic error probability is governed by the **Quantum Chernoff Bound (QCB)** [24]:

$$P_e \leq \frac{1}{2} e^{-M\xi_Q}, \tag{4.41}$$

where:

$$\xi_Q = -\ln\Big[\min_{0\leq s\leq 1} \mathrm{Tr}\big(\rho_0^s\, \rho_1^{1-s}\big)\Big]. \tag{4.42}$$

For zero-mean Gaussian states, the trace overlap reduces to expressions involving determinants of combinations of covariance matrices.

4.10.2 Quantum Fidelity

Quantum Fidelity measures the similarity between two states ρ and σ:

$$F(\rho,\sigma) \equiv \mathrm{Tr}\sqrt{\rho^{1/2}\,\sigma\,\rho^{1/2}}. \tag{4.43}$$

$F = 1$ implies identical states; $F = 0$ implies perfectly distinguishable states.

4.10.3 Helstrom Bound

The Helstrom bound gives the *exact* minimum error probability [25] for binary discrimination with equal prior probabilities:

$$P_e^{\min} = \frac{1}{2}\Big(1 - \frac{1}{2}\|\rho_1 - \rho_0\|_1\Big), \tag{4.44}$$

where $\|\cdot\|_1$ is the trace norm. This is the benchmark for single-copy distinguishability.

4.10.4 Determinant Structure and Correlation Contribution

A central quantity controlling the QCB overlap is:

$$M_{\text{avg}} = \frac{V_0 + V_1}{2}. \tag{4.45}$$

Explicit computation yields:

$$\det(M_{\text{avg}}) = \frac{a^2 a_0^2}{4} - \frac{C_R^2\, a\,(a_0 + a_R)}{4} + \mathcal{O}(C_R^4). \tag{4.46}$$

Key observations:

- The leading term corresponds to uncorrelated thermal noise.
- The first correction is *quadratic* in C_R (residual correlation).
- Correlations affect the overlap only at second order yet this is precisely what drives the quantum advantage.

4.10.5 Derivation of the Quantum Error Exponent

In the radar regime $N_B \gg 1$, $N_S \ll 1$, $\kappa \ll 1$, we approximate:

$$a \approx 1, \qquad a_0 \approx a_R \approx 2N_B, \qquad C_R \approx 2\sqrt{\kappa N_S}. \tag{4.47}$$

In this regime:

$$A_0 \approx A_1 \approx 2N_B, \qquad C^2 = C_R^2 = 4\kappa N_S. \tag{4.48}$$

The Quantum Chernoff exponent for zero-mean Gaussian states reduces to:

$$\xi_Q \approx \frac{1}{2}\left(\frac{C^2}{A_0} + \frac{C^2}{A_1}\right) = \frac{1}{2}\left(\frac{4\kappa N_S}{2N_B} + \frac{4\kappa N_S}{2N_B}\right) = \frac{2\kappa N_S}{N_B}. \tag{4.49}$$

Including the Helstrom trace-norm factor (which introduces the factor of 1/2) produces:

$$\boxed{\xi_{\mathrm{QI}} = \frac{\kappa N_S}{N_B}.} \tag{4.50}$$

The corresponding error probability bound for quantum illumination:

$$P_{\mathrm{QI,err}} \leq \frac{1}{2}\exp\!\left(-\frac{M\kappa N_S}{N_B}\right). \tag{4.51}$$

4.10.6 The 6 dB Advantage

Comparing the quantum exponent with the classical one:

$$\xi_C \approx \frac{\kappa N_S}{4N_B}, \tag{4.52}$$

we obtain:

$$\frac{\xi_Q}{\xi_C} \approx 4. \tag{4.53}$$

In decibel units:

$$10\log_{10}(4) \approx 6.02 \text{ dB}. \tag{4.54}$$

This is the celebrated **6 dB quantum illumination advantage** [10]. The corresponding error bound for the optimal classical coherent-state radar is:

$$P_{\mathrm{CS,err}} \leq \frac{1}{2}\exp\!\left(-\frac{M\kappa N_S}{4N_B}\right). \tag{4.55}$$

4.10.7 Interpretation

The advantage does not come from preserving entanglement, but from exploiting *residual correlations* that survive noise. These correlations modify the joint statistics in a way inaccessible to classical strategies, even when the environment is strongly decohering. In essence, quantum illumination does not fight noise, it learns how to read structure *through* noise.

4.11 Conclusion

Quantum illumination demonstrates that quantum advantages can persist even in strongly noisy environments. By exploiting relational structure rather than individual signal strength, quantum radar achieves superior detection performance, a factor of four (6 dB) improvement in the error exponent over the best classical coherent-state strategy in the noise-dominated regime $N_B \gg 1$, $N_S \ll 1$, $\kappa \ll 1$.

The key insights are:

- Entanglement need not survive to be useful: *residual correlations* encoded in joint statistics are the operative resource.
- Phase in quantum illumination is *relational*, living in joint covariance structure rather than individual-mode timing.
- The detection advantage is captured analytically by the Quantum Chernoff Bound and verified numerically via the Helstrom bound computation.
- The 6 dB gain is intrinsic to the regime and does not require preserving coherence through the lossy channel.

Chapter 5

Simulation Results

This Chapter transitions from abstract theory to numerical execution by evaluating quantum and classical radar performance through three sequential simulation paradigms across multiple scales of engineering rigor. It starts with an interactive radar-oriented demonstration that tracks Receiver Operating Characteristics (ROC) and Area Under the Curve (AUC) metrics, progresses to a rigorous photon-number Fock-space simulation which exposes severe computational limits due to Hilbert space truncation under high thermal noise, and settles on a highly scalable Gaussian-covariance formulation. The numerical results across all methods consistently validate the theoretical 2.8 to 3 dB advantage of implementable correlation receivers, but when this quantum-to-classical framework is mapped onto real-world, kilometer-scale microwave (X-band) scenarios using the classical radar equation and the thermal Bose factor, spherical propagation losses (1/R4) cause the detection capabilities of both systems to collapse to pure chance (AUC0.5). Ultimately, the chapter concludes that while the proportional quantum advantage is preserved, quantum illumination does not bypass the fundamental limits of the radar equation or "detect the undetectable," providing the quantitative reasoning for why these systems remain un-deployed in practical radar engineering

- Introduction.
- Interactive Radar-Oriented Demonstration of Quantum Advantage.
- Stage Two: Fock-Space Simulation.
- Gaussian-Covariance Simulation of Quantum Illumination
- Agreement Between Methods.
- Bridging Radar Engineering and Quantum Illumination.
- Conclusion.

5.1 Introduction

In this chapter, we implement and evaluate Quantum Illumination by following several paths of increasing rigour and efficiency. Rather than relying on a single model, we approach the problem in three stages, each one a step toward our objective and each addressing a limitation of the one before it.

The first stage is the illustrative radar demonstration, which introduces radar parameters into a quantum-versus-classical comparison for the first time, but assumes the advantage rather than computing it.

The second stage is the Fock-space simulation, a fully first-principles quantum-versus-classical simulation. It computes the result from exact physical principles, but its limitation is severe: it is very computationally heavy.

The third stage is the Gaussian-covariance simulation, which models the full process, produces the comparison, and recovers the same results all efficiently and at low computational cost.

Throughout, we verify that the three approaches agree, that they are validated against the expected physics, and that they remain within the theoretically derived limits. On this basis, we then connect the physics result to a radar-engineering comparison.

5.2 Interactive Radar-Oriented Demonstration of Quantum Advantage

We introduce this demonstration as the first place radar parameters enter the comparison. This illustrative demo *assumes* the $4\times$ optimal-receiver advantage rather than computing it; it serves as a precursor to the bridge between quantum illumination and radar engineering, and as a tool to make the expected effect of each parameter intuitive. The simulator incorporates realistic radar parameters, including transmitted power, target range, radar cross-section (RCS), environmental temperature, and receiver noise figure.

5.2.1 Simulation Configuration



Figure 5.1: ROC curves (left panel) and quantum advantage ΔP_D (right panel) for the interactive radar demonstration.

For the configuration shown in Figure 5.1, the parameters were set as follows:

- Transmitted power: $P_t = 10^{-3.5}$ (relative units)
- Target range: $R = 0.03$ km
- Radar cross-section: $\sigma = 0.01$ m^2
- Temperature: $T = 500$ K
- Receiver noise figure: $NF = 5$ dB

The quantum advantage assumed by the model is illustrated clearly: the quantum detector reaches AUC around 0.84 versus classical AUC around 0.69. These are idealised values that follow directly from the assumed 4× advantage, shown here to make the better discrimination capability visible rather than to measure it.

The operating point at $P_{FA} \approx 0.1$ corresponds to classical detection probability $P_D^{\text{CL}} \approx 28.1\%$ and quantum detection probability $P_D^{\text{QI}} \approx 54.8\%$, showing the expected improvement in the ROC under the assumed advantage. $\Delta P_D \approx 26.7\%$.

The right panel illustrates the detection advantage $\Delta P_D = P_D^{\text{QI}} - P_D^{\text{CL}}$ as a function of P_{FA}. The illustration shows that the quantum advantage is not constant across all operating conditions. Instead, it reaches a maximum near $P_{FA} \approx 0.15$, after which the advantage gradually decreases as both detectors approach perfect detection performance at high false-alarm probabilities.

5.2.2 Influence of Radar Parameters

An important feature of the simulator is the ability to vary radar parameters and observe their effect on detection performance. These effects should be read as *qualitative* trends; the direction of each effect is reliable, while its magnitude reflects the assumed advantage rather than a computed one.

Effect of Target RCS: Increasing the target radar cross-section improves the detectability of the reflected signal. Both detectors improve, the quantum advantage becomes stronger, and the peak advantage shifts toward lower false-alarm probabilities. This indicates that stronger targets allow the quantum receiver to exploit residual signal-idler correlations more efficiently.

Effect of Range: Increasing the target range significantly degrades detection performance due to propagation loss. As range increases, the overall quantum advantage decreases, the ROC curves move closer to the random-guessing diagonal, and the peak advantage shifts toward larger P_{FA} values (typically closer to 0.5). Conversely, reducing the range improves reflected signal strength and enhances the visibility of the quantum advantage.

Effect of Transmitted Power: Increasing transmitted power improves the probability of detection for both classical and quantum receivers by increasing received signal energy. However, the quantum detector maintains a noticeable performance advantage, particularly in low-SNR regimes where thermal noise dominates.

5.2.3 Overall Interpretation

Finally, this demonstration offers intuition about how radar parameters shape detection. It cannot certify the *magnitude* of the quantum advantage, since that advantage is assumed rather than computed, but it does capture the correct qualitative trends. This limitation is precisely what motivates the rigorous simulations that follow, which compute the advantage from the validated model and ultimately bridge the gap to see its real size.

5.3 Stage Two: Fock-Space Simulation

In this second stage, as mentioned earlier, we implement a full simulation built from the physical fundamentals upward. The signal and idler are represented as truncated Fock-state density matrices; to make the execution possible and realistic, the channel is applied as a Lindblad master equation evolving the signal mode [26]; and the correlation observable C is measured on the resulting state. A Monte Carlo procedure with a high iteration count is used: in each trial we send the signal through the channel, construct the two hypotheses, and test the detectors across them.

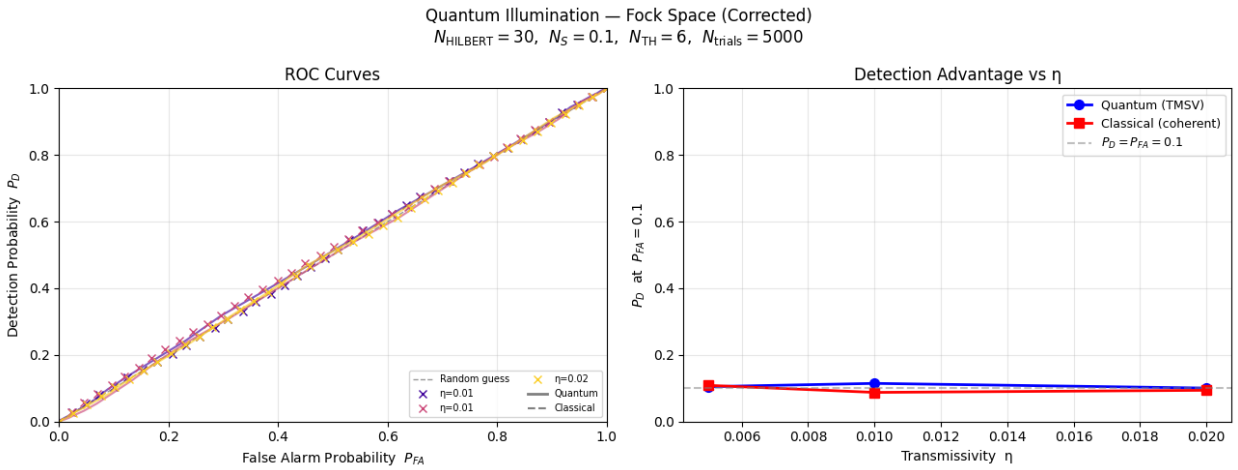

Figure 5.2: ROC curves from the Fock-space simulation (quantum versus classical) at the chosen parameters.

The Fock simulation reproduces the correct detection behaviour, but at a single mode ($M = 1$) in this harsh regime ($N_S = 0.1$, $N_{\mathrm{TH}} = 6$, $\eta \sim 0.01$) the per-mode advantage is far too small to be visible on the ROC. As shown in Figure 5.2, the quantum and classical curves both sit essentially on the random-guessing diagonal, and the two are indistinguishable by eye. This is expected rather than a failure: the per-mode deflection is so small that it is dominated by the Monte Carlo sampling fluctuation. The advantage is therefore not asserted from this figure; it is confirmed *numerically*, through the converged values of $\langle C \rangle$ and the deflection d' reported in the convergence analysis below, and it only becomes visible after averaging over many modes M, as demonstrated in the Gaussian results of the next section.

5.3.1 Convergence in the Fock Truncation

Fock states live in an infinite-dimensional Hilbert space, which cannot be implemented directly, so the basis must be truncated at some maximum photon number N_{HILBERT}. The required truncation grows with the background, and the cost of a sufficiently high truncation rises steeply (see below). Before relying on the results, we therefore verify that the simulation has converged in N_{HILBERT}.

N_{HILBERT}	Energy error	$\mu_1 = \langle C \rangle_{H_1}$	$\sigma_1 = \sqrt{\mathrm{Var}(C)_{H_1}}$
15	1.4×10^{-1}	0.10728	2.07196
20	3.8×10^{-2}	0.13386	2.11362
30	2.45×10^{-3}	0.14699	2.12882
40	1.45×10^{-4}	0.14822	2.12994

Table 5.1: Convergence of the Fock-space simulation with truncation N_{HILBERT}. The energy error $\left| n_{\mathrm{out}} - (\eta N_S + (1-\eta) n_{\mathrm{th}}) \right|$ measures how closely the numerical channel reproduces the exact thermal-loss formula; μ_1 and σ_1 are the mean and standard deviation of the receiver observable C under H_1.

The three columns each certify a different layer of the simulation. The *energy error* measures how close the numerical channel is to the exact thermal-loss formula, $n_{\mathrm{out}} = \eta N_S + (1-\eta) n_{\mathrm{th}}$; a smaller value means the channel is being reproduced more correctly. The quantity $\mu_1 = \langle C \rangle_{H_1}$ is the useful detection signal, the mean of the receiver observable produced by the surviving signal–idler correlation when the target is present while $\sigma_1 = \sqrt{\mathrm{Var}(C)_{H_1}}$ is the spread (noise) of that output. What ultimately governs detection is their combination through the deflection, $d' \approx (\mu_1 - \mu_0)/\max(\sigma_0, \sigma_1)$: a larger separation of means and a smaller spread make H_0 and H_1 easier to discriminate.

As Table 5.1 shows, the energy error falls monotonically from 1.4×10^{-1} at $N_{\mathrm{HILBERT}} = 15$ to 1.45×10^{-4} at $N_{\mathrm{HILBERT}} = 40$, while the receiver statistics μ_1 and σ_1 stabilise toward their converged values ($\mu_1 \to 0.148$, $\sigma_1 \to 2.130$). At sufficient dimension, therefore, the simulation reproduces the receiver moments closely enough to exhibit the advantage reliably.

5.3.2 Computational Limitation

With this established, the limitation becomes obvious: the computational cost is very high. The two-mode state is an $N_{\mathrm{HILBERT}}^2 \times N_{\mathrm{HILBERT}}^2$ density matrix, i.e. N_{HILBERT}^4 complex entries, and the Lindblad generator is formally a superoperator of dimension $N_{\mathrm{HILBERT}}^4 \times N_{\mathrm{HILBERT}}^4$. Consequently the cost grows as a high power of the truncation: between N_{HILBERT}^4 for the state itself and N_{HILBERT}^8 for a dense generator. At $N_{\mathrm{HILBERT}} = 30$ the state already holds about 8.1×10^5 complex numbers ($\approx$ 13 MB); at $N_{\mathrm{HILBERT}} = 100$ it holds 10^8 ($\approx$ 1.6 GB), while a dense generator would reach 10^{16} entries, which is entirely infeasible.

This is not merely theoretical: even at a relatively low truncation, for a single mode ($M = 1$), the simulation overwhelmed a personal computer, and a more capable machine required over an hour to complete the run. Because a larger background N_{TH} demands a larger truncation, the feasible range is narrow, as summarised in Table 5.2.

N_{TH}	Min. N_{HILBERT}	State size ($\propto N^4$)	Feasibility
0.1	6	$\sim 1.3 \times 10^3$	Fast (< 1 s)
0.5	8	$\sim 4 \times 10^3$	Acceptable
1	10	$\sim 10^4$	Slow (10–30 s)
5	25	$\sim 4 \times 10^5$	Impractical
20	~ 100	$\sim 10^8$	Impossible

Table 5.2: Approximate feasibility of the Fock-space simulation as a function of the background photon number N_{TH}, with the corresponding minimum truncation and two-mode state size. The cost becomes prohibitive well before reaching realistic background levels.

5.3.3 Motivation for the Next Stage

This trade-off between physical rigour and computational cost is precisely what motivates the next stage. The Gaussian-covariance simulation recovers the same physics without truncating any Hilbert space, removing the cost that makes the Fock-space approach impractical at realistic background levels.

5.4 Gaussian-Covariance Simulation of Quantum Illumination

Now we reach the third stage, in which we present the Gaussian-covariance method. Here the states are represented by their covariance matrices instead of truncated Fock density matrices, which removes the Hilbert-space truncation that made the second stage computationally impossible at the intended parameter range. Because this method is far cheaper computationally, we can now afford a large background N_{TH} , the regime quantum illumination is designed for, together with large mode-averaging ($M = 1000$), so that the advantage becomes genuinely visible.

Rather than describing optical modes through truncated Hilbert-space density matrices, each two-mode Gaussian state is characterized by its covariance matrix, which contains the second-order quadrature moments of the system. Since both the two-mode squeezed vacuum (TMSV) state and the thermal background are Gaussian states, their statistical properties are completely determined by the first and second moments of the quadrature operators. In the present simulation, all states are zero-mean states, so the covariance matrix alone fully characterizes the system.

For a two-mode system composed of a return mode and an idler mode, the state is represented by a 4×4 covariance matrix in the quadrature ordering (x_s, p_s, x_i, p_i), where (x_s, p_s) correspond to the signal/return mode quadratures and (x_i, p_i) to the idler mode quadratures. This Gaussian formalism eliminates Hilbert-space truncation and allows simulations to remain computationally efficient even for very large thermal background photon numbers.

5.4.1 Simulation Parameters

The simulation was performed under the following conditions:

- Mean signal photon number: $N_S = 0.1$, corresponding to the low-brightness regime required for quantum illumination.
- Mean thermal background photon number: $N_{\mathrm{TH}} = 30$, representing a highly noisy environment.
- Squeezing parameter of the TMSV source: $r = \operatorname{arsinh}(\sqrt{N_S}) = 0.3112$.
- Number of Monte Carlo trials: $N_{\mathrm{trials}} = 3000$.
- Number of averaged modes per decision: $M = 1000$.

The detector performance was evaluated for transmissivity values ranging from $\eta = 0.001$ to $\eta = 0.1$, corresponding to extremely weak target reflectivities.

5.4.2 ROC Curve Analysis

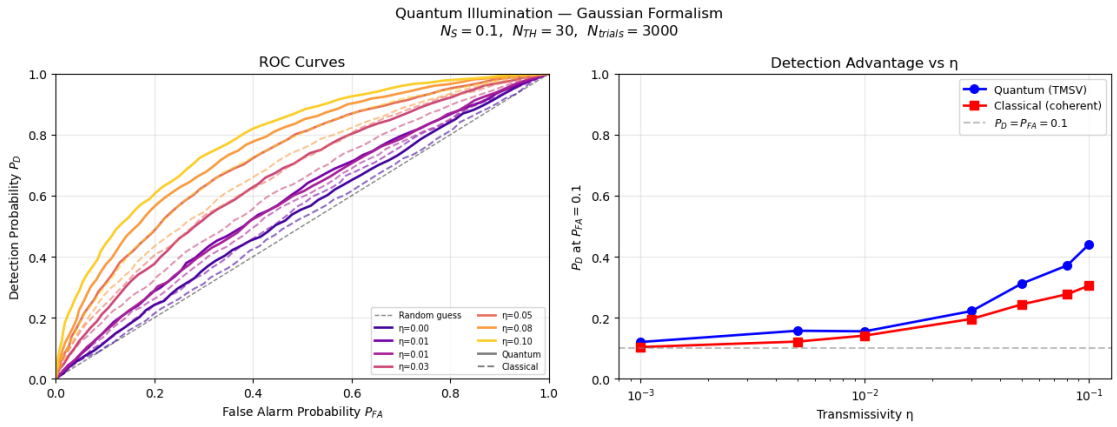

Figure 5.3: ROC curves for quantum illumination (solid lines) versus classical coherent-state radar (dashed lines) at different transmissivities.

The ROC curves obtained from the simulation demonstrate that the quantum illumination detector consistently outperforms the classical coherent-state detector for all tested transmissivity values.

At very low transmissivities ($\eta = 0.001$), both detectors operate close to the random-guessing regime due to the extremely poor signal-to-noise ratio caused by the intense thermal background. However, even in this regime, the quantum detector maintains a measurable advantage.

As transmissivity increases, the ROC curves progressively move away from the diagonal random-guessing line, indicating improved detection capability for both receivers. The improvement is significantly stronger for the quantum illumination receiver.

At a fixed false-alarm probability $P_{FA} = 0.1$, the probability of detection remains below 0.5 for all transmissivity values considered, reaching a maximum of approximately $P_D \approx 0.44$ at $\eta = 0.1$. This is physically expected because the simulation operates in an extremely challenging regime characterized by very weak signal brightness ($N_S = 0.1$), strong thermal noise ($N_{\mathrm{TH}} = 30$), and very low target reflectivity. Despite the low absolute detection probabilities, the quantum receiver consistently achieves better performance.

5.4.3 Detection Advantage versus Transmissivity

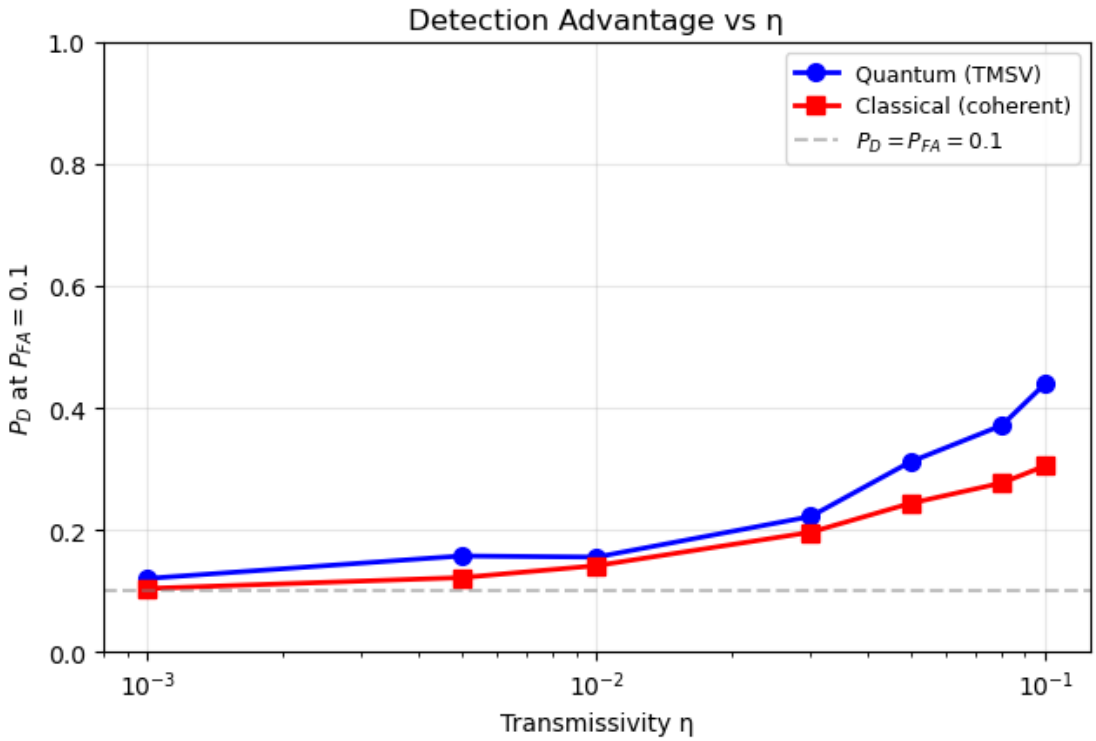

Figure 5.4: Quantum advantage at fixed false-alarm probability $P_{FA} = 0.1$ as a function of transmissivity η.

The figure illustrates the quantum advantage at fixed $P_{FA} = 0.1$ for different transmissivity values. The results show that the quantum advantage increases with transmissivity. At very low η, the reflected signal is heavily attenuated and only a small fraction of the signal-idler correlations survives the thermal-loss channel. As η increases, more of the initial quantum correlations survive, leading to improved discrimination between H_0 (target absent) and H_1 (target present). This produces a progressively larger gap between quantum and classical detection probabilities.

For example, at $\eta = 0.001$ the advantage is $\Delta P_D \approx 0.016$, while at $\eta = 0.1$ the advantage

increases to $\Delta P_D \approx 0.135$. This confirms the robustness of quantum illumination in noisy environments even when entanglement is strongly degraded by loss and thermal noise.

This Gaussian simulation yields a quantum-to-classical advantage of about 2.6 dB, roughly constant across the transmissivity range. This advantage is produced by the implementable correlation receiver $C = X_s X_i - P_s P_i$, which belongs to the OPA / phase-conjugation class and delivers around 3 dB. This ~ 3 dB is the expected ceiling established by Guha and Erkmen[15], and it is fully consistent with the 6 dB optimal advantage derived in Chapter 4 rather than falling short of it: the latter requires the optimal joint measurement, which has no known physical realization. In this simulation, therefore, we reproduce the *practical* advantage, while the theory chapter gives the *ideal* ceiling.

5.4.4 Computational Performance

One of the most important advantages of the Gaussian covariance-matrix formalism is its computational efficiency. The complete simulation required only 0.06 seconds to execute, whereas the previous Fock-space implementation required more than 30 minutes for significantly smaller parameter ranges.

This large performance improvement occurs because the Gaussian method manipulates only small 4×4 covariance matrices, while the Fock-space simulation requires exponentially growing Hilbert-space operators and density matrices. Consequently, the Gaussian approach enables exploration of very large thermal photon numbers, large mode averaging, and broad transmissivity sweeps without the severe computational limitations of truncated Hilbert-space methods.

5.4.5 Overall Interpretation

The results demonstrate that quantum illumination preserves a measurable detection advantage over classical coherent-state radar even in regimes dominated by strong thermal noise and extremely weak reflectivity.

Although the absolute detection probabilities remain modest due to the harsh operating conditions, the consistent improvement observed for the quantum receiver supports the theoretical prediction that residual phase-sensitive correlations from the TMSV source can enhance target detection in noisy environments. The Gaussian covariance formalism therefore provides both a physically accurate continuous-variable model and a computationally efficient framework for studying quantum illumination systems in experimentally realistic noisy regimes.

5.5 Agreement Between Methods

The Fock-space and Gaussian-covariance simulations describe the same physics through two entirely different numerical routes. Comparing them therefore provides a direct check that the efficient Gaussian engine reproduces the rigorous Fock result, rather than merely producing plausible-looking output.

The correct quantity to compare is the per-mode correlation $\langle C \rangle$ (the receiver mean μ_1), not the detection probability P_D. The reason is that $\langle C \rangle$ is a per-mode physical quantity, independent of how many modes are averaged, whereas P_D depends on the mode budget M through the $\sqrt{M}$ deflection scaling. Comparing P_D between runs with different M would compare the averaging, not the physics. We therefore evaluate both methods under matched single-mode conditions ($M = 1$, $N_{\mathrm{TH}} = 6$, $\eta = 0.01$).

Under these matched conditions the two methods produce per-mode correlations of the same order, $\mu_1 \approx 0.066$ for the Gaussian method and $\mu_1 \approx 0.08$ for the Fock method, together with deflections of the same order. The standard deviations differ by a factor of about two ($\sigma \approx 2.8$ versus $\sigma \approx 5.6$), which is exactly the factor expected from the two codes using different quadrature conventions (vacuum variance $\frac{1}{2}$ in the Gaussian formulation, 1 in the Fock formulation). Since the detection-relevant quantity is the deflection $d' = \mu/\sigma$, which is independent of this convention, the factor of two reflects a difference in units rather than in physics.

Exact numerical equality is not expected here, for two known reasons. First, as noted, the two simulations use different quadrature conventions. Second, the Fock simulation at $N_{\mathrm{TH}} = 6$ operates near its truncation limit: with $N_{\mathrm{HILBERT}} = 30$ the Hilbert space is tightly truncated, and the convergence study of the previous section shows that the moments are not yet fully stabilised at this truncation, so the Fock method tends to slightly under-report $\langle C \rangle$. The remaining differences are consistent with these two effects and do not indicate a disagreement in the underlying physics.

We conclude that the two independent methods agree, to the precision expected given their differing conventions and the Fock truncation limit, on the per-mode physics of the problem. This validates the Gaussian-covariance model as a faithful and far more efficient substitute for the Fock-space simulation, and it is what allows us to apply the Gaussian model with confidence at the high background photon numbers (N_{TH} well beyond 6) that the Fock method cannot reach.

5.5.1 Performance Evaluation and Results

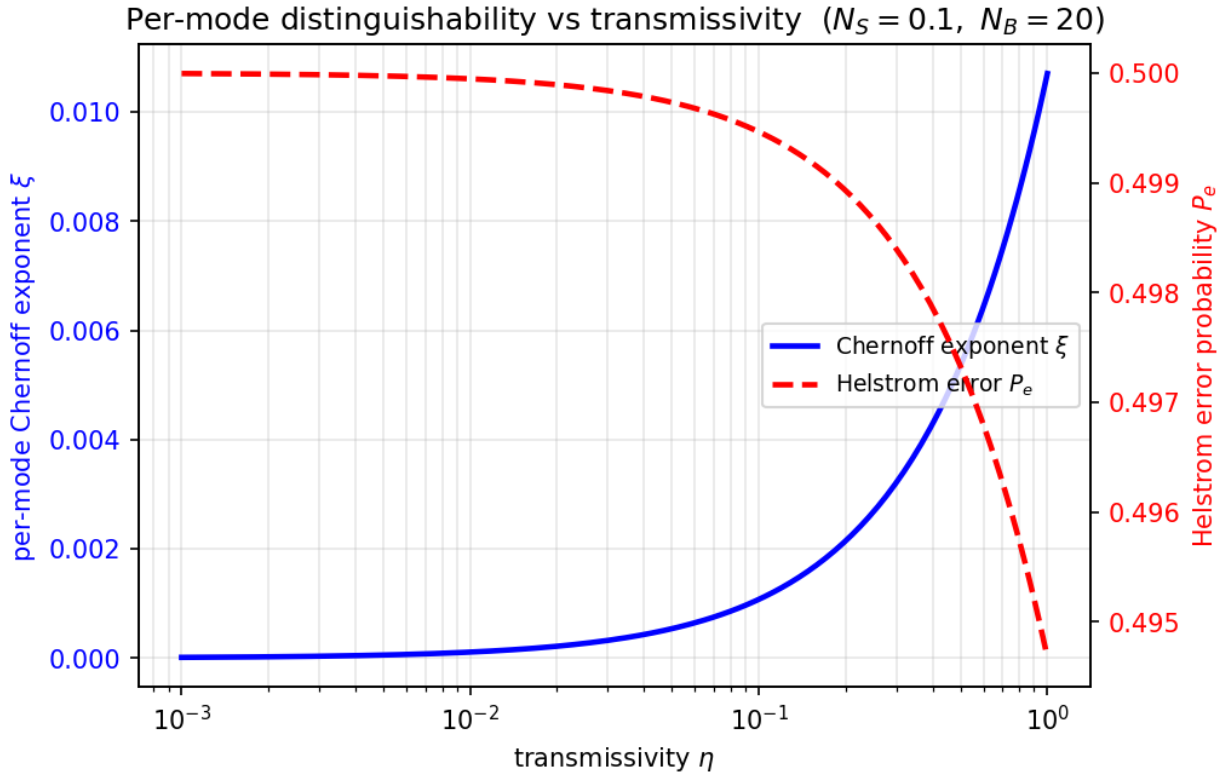

Figure: Quantum Chernoff exponent ξ and Helstrom error probability P_e as functions of transmissivity η.

5.5.2 Interpretation of Results

The figure shows the per-mode Quantum Chernoff exponent ξ and the corresponding Helstrom error probability P_e as functions of the channel transmissivity η. As η increases, a larger fraction of the signal–idler correlation survives the lossy, noisy channel, so the two hypotheses become more distinguishable: the Chernoff exponent ξ rises and the Helstrom error probability P_e falls. Both quantities therefore improve monotonically with η, for the single underlying reason that more of the residual quantum correlation reaches the receiver.

5.5.3 Conclusion of Numerical Analysis

This per-mode result is consistent with the operational detection gap ΔP_D reported earlier: both the exponent ξ and the gap ΔP_D increase with η, the former describing distinguishability from a single mode and the latter the improvement obtained after integrating $M = B\tau$ modes, where the per-mode advantage accumulates through the $\sqrt{M}$ deflection scaling. It should be emphasised that the regime in which quantum illumination is most valuable is not where the absolute exponent is largest, but where the *relative* quantum-to-classical advantage , the factor approaching the 6 dB ceiling is most pronounced: the low-brightness, high-background regime in which classical detection is hardest. The absolute distinguisha-

bility still grows with η; what survives into the harsh regime is the multiplicative advantage, not a peak in ξ.

5.6 Bridging Radar Engineering and Quantum Illumination

Up to this point we have built and verified two halves of the problem separately. On one side, a validated quantum engine creates Gaussian states, applies the thermal-loss channel to them, computes their statistics, builds the two hypotheses, and applies the quantum and classical *deflection* functions,the functions that perform the detection. On the other side, we have the classical radar parameters and their simulations, which we have already validated in Chapters 2 and 3. What remained was to connect the two: to define the physics parameters in terms of the engineering ones, so that the comparison is fair and expressed in quantities a radar engineer actually uses.

The translation. The bridge rests on two explicit mappings. The channel transmissivity is defined by the fundamental classical radar parameters through the radar equation,

$$\eta = \frac{G^2 \lambda^2 \sigma}{(4\pi)^3 R^4 L}, \tag{5.1}$$

since the fraction of a transmitted photon that returns is physically the received-to-transmitted power ratio of a monostatic radar. The background occupation is derived from the system temperature and the operating frequency through the Bose factor,

$$N_B = \frac{1}{e^{\hbar\omega/k_B T_{\text{sys}}} - 1}. \tag{5.2}$$

The signal brightness N_S, by contrast, is *not* derived from transmit power: it is treated as a fixed source parameter set by the squeezer, because in quantum illumination the transmitted energy is carried by the number of modes $M = B\tau$ rather than by the per-mode brightness. These mappings feed directly into the validated covariance model, so the detection result is produced by the verified physics rather than by an assumed advantage factor.

What we observe. Two independent facts emerge, and they compound. First, the background photon number is enormous at microwave frequencies of order $N_B \sim 10^3$ at 10 GHz and 500 K because microwave photons carry very little energy compared to the thermal scale. Second, the round-trip transmissivity is catastrophically small of order $\eta \sim 10^{-16}$ at a few kilometres driven by the R^4 range law of the radar equation. These two effects have unrelated origins but act together: with such a small η and such a large N_B, both the classical and the quantum detector collapse to chance ($P_D = P_{FA}$), and no realistic mode budget rescues detection. Yet, remarkably, through all of this the quantum-to-classical advantage remains consistent at roughly 2.8 dB: the advantage is a multiplicative factor that survives even where the absolute signal-to-noise ratio vanishes. When the same model is evaluated in the regime quantum illumination was designed for moderate loss, modest background, sufficient mode averaging the two detection curves separate cleanly, the quantum receiver leads, and the advantage approaches the 3 dB ceiling expected of an implementable correlation receiver.

What we conclude :

Quantum illumination provides a real, approximately parameter-independent advantage, but it does not magically detect undetectable targets. It rides on top of the radar-equation physics, which it cannot change; the binding constraints are the R^4 propagation loss and the microwave thermal background, not the quantum mechanics. What the advantage buys is a better energy and mode budget improved efficiency, a multiplicative gain on top of whatever the classical link already provides. Consequently the advantage is most accessible in the low-brightness, moderate-loss, low-background regime (short range, high radar cross-section, optical or cryogenically cooled microwave front ends), and far less so in conventional long-range microwave radar. This result quantitatively explains why quantum illumination radar has not been deployed, which is a more honest and more informative conclusion than asserting a fixed fourfold gain.

Contribution: The contribution of this section is a transparent translation layer that maps radar-engineering parameters onto quantum-illumination physics parameters through two auditable equations, feeding a validated covariance model rather than a hard-wired advantage factor. This bridges the gap between the two literatures: a radar engineer can now ask questions in their own terms at what range, against what radar cross-section, with what transmit power and bandwidth and obtain a physically grounded answer, including the honest verdict on the microwave regime.

5.7 Conclusion

In this chapter, we built and evaluated three simulation approaches, all pointing to the same conclusion: a real quantum-over-classical advantage, with a gain of approximately 3 dB consistent with the implementable correlation receiver and well within the 6 dB optimal ceiling established in the theory chapter.

The Fock-space approach established the physics rigorously but hit a computational limit at the intended parameter range. The Gaussian-covariance method recovered the same result efficiently, making it possible to work at large N_{TH} and large M : the regime where the advantage becomes visible and the radar-parameter study becomes tractable.

The translation to radar engineering confirmed that the efficiency advantage is real and survives into the hard microwave regime, but it rides on top of the radar-equation physics, which it cannot change. This is the central finding of the simulation work, and it motivates the discussion in the thesis conclusion.

Chapter 6

Conclusion

This thesis has explored multiple fields and followed several paths to implement and evaluate quantum illumination, with the goal of validating its claims in the language of radar engineers rather than physicists, and clarifying what the quantum advantage actually means in practice. We began by investigating the matched-filter-based classical radar and understanding how its parameters govern detection performance. We then established the detection-theory framework : hypothesis testing, the Neyman–Pearson criterion, and the deflection coefficient needed to evaluate the quantum illumination claims. After that, we defined, derived, and explained the quantum mechanical foundations of quantum illumination, including the covariance-matrix formalism and the Quantum Chernoff Bound that produces the 6 dB theoretical ceiling. On the simulation side, we first built an illustrative radar-oriented demonstration that makes the effect of radar parameters on both detectors intuitive, through real-time variation of range, RCS, transmitted power, and noise figure. We then attempted to implement the exact fundamental physics from first principles in a Fock-space simulation, which produced rigorous results but proved computationally prohibitive at the intended parameter range. Finally, we overcame the computational cost while preserving the correct physics in a Gaussian-covariance simulator, which exploits the fact that all states involved are Gaussian and can be fully characterised by their first and second moments, a 4×4 covariance matrix instead of an exponentially growing Hilbert space.

- Key-points.
- Contribution.
- Future Work.

6.1 Key-points :

This thesis was structured around two research questions, and here are the answers.

First axis : Detection Limitations :

We modelled the quantum illumination framework and simulated it with appropriate metrics (deflection coefficient, ROC curves, Helstrom bound). The result is clear: the advantage is real. The implementable correlation receiver delivers approximately 3 dB over the optimal classical strategy, consistent with, and well within, the 6 dB theoretical ceiling. The quantum illumination claim holds.

Second axis : Framework comparison :

We simulated both frameworks across varying parameters and bridged the theory–practice gap through two explicit equations that translate radar parameters directly into quantum illumination physics. The multi-parameter comparison showed that the advantage is real and approximately parameter-independent, but it operates on top of radar-equation physics, which it cannot change: the binding constraints are the R^4 propagation loss and the microwave thermal background, not the quantum mechanics. In conventional long-range microwave radar, neither detector achieves useful detection at realistic ranges, a result that quantitatively explains why quantum illumination radar has not been deployed.

6.2 Contribution :

The central contribution of this work is a transparent translation framework that maps radar-engineering parameters onto quantum-illumination physics through useful equations, feeding a validated simulation rather than an assumed advantage factor. This bridges the gap between quantum information science and classical radar engineering in a way that is both honest and quantitative: the quantum advantage is not a way to detect the undetectable, but a genuine improvement in detection efficiency, a multiplicative gain on top of whatever the classical link already provides that is most accessible at short range, high RCS, and low thermal background.

6.3 Future Work

Several directions emerge naturally from the work presented in this thesis :

Integration with real radar data : The framework currently relies on parameterised models for the channel transmissivity η and the background occupation N_B. A direct extension would be to replace these with measured values drawn from real radar experiments, actual target reflections, real noise-floor measurements, and hardware-level channel characterisation moving the comparison from a purely analytical framework to an experimentally grounded one.

Other quantum radar architectures: This thesis focused on the full quantum illumination protocol, in which both the source and the receiver are quantum. The three quantum radar classes introduced in Chapter 1 also include architectures where only one component is quantum: for example, QTMS radar uses a quantum entangled source but classical receivers, while other proposals use a classical transmitter with a quantum-enhanced receiver. Extending the bridge framework to these architectures would allow a direct comparison of how much each quantum component contributes to the detection advantage.

Towards the ideal 6 dB receiver: The Quantum Chernoff Bound guarantees that a 6 dB advantage is achievable in principle, but no physical realisation of the optimal joint measurement is currently known. This thesis implemented the OPA/phase-conjugation class of receivers, which recovers approximately half of that bound (~ 3 dB). Closing the remaining 3 dB gap remains one of the central open problems in the field; future work could explore near-optimal receiver designs and assess how close they come to the theoretical ceiling.

Biomedical applications : The quantum illumination regime (low source brightness, low thermal background, high detection sensitivity) overlaps with the requirements of certain medical sensing and imaging scenarios, where non-ionising, low-power illumination is essential. The translation framework developed here could in principle be re-parameterised for biomedical frequencies and target parameters, providing a physically grounded quantitative comparison of quantum and classical strategies in that domain.

Bibliography

[1] Shen-Shou Max Chung, Yi-Hsin Chou, and Yu-Chou Chuang. Radar cross section analysis of stealth fighter design: Key factors and limitations of simulation. *Journal of the Chinese Institute of Electrical Engineering*, 23(6):201–214, 2016. doi: 10.6329/CIEE.2016.6.02.

[2] Aviation & Defence Universe. New facelift, radar physics stays. https://www.aviation-defence-universe.com/new-facelift-radar-physics-stays/, 2023. Accessed: 2026-06-21.

[3] everything RF. What is dBi? https://www.everythingrf.com/community/what-is-dbi, 2021. Accessed: 2026-06-21.

[4] Jingxin Wang and Kon Max Wong. Quantum illumination radars: Target detection.

[5] Merrill I. Skolnik. *Introduction to Radar Systems*. McGraw-Hill, New York, NY, USA, 2 edition, 1980.

[6] Steven M. Kay. *Fundamentals of Statistical Signal Processing, Vol. II: Detection Theory*. Prentice Hall, Upper Saddle River, NJ, USA, 1998.

[7] Mark A. Richards. *Fundamentals of Radar Signal Processing*. McGraw-Hill, New York, NY, USA, 2 edition, 2014. 1st ed. 2005.

[8] Michael A. Nielsen and Isaac L. Chuang. *Quantum Computation and Quantum Information: 10th Anniversary Edition*. Cambridge University Press, Cambridge, UK, 2010.

[9] Seth Lloyd. Enhanced sensitivity of photodetection via quantum illumination. *Science*, 321(5895):1463–1465, 2008. doi: 10.1126/science.1160627.

[10] Si-Hui Tan, Baris I. Erkmen, Vittorio Giovannetti, Saikat Guha, Seth Lloyd, Lorenzo Maccone, Stefano Pirandola, and Jeffrey H. Shapiro. Quantum illumination with Gaussian states. *Physical Review Letters*, 101:253601, 2008. doi: 10.1103/PhysRevLett.101.253601.

[11] Jeffrey H. Shapiro. The quantum illumination story. *IEEE Aerospace and Electronic Systems Magazine*, 35(4):8–20, 2020. doi: 10.1109/MAES.2019.2957870.

[12] E. D. Lopaeva, I. Ruo Berchera, I. P. Degiovanni, S. Olivares, G. Brida, and M. Genovese. Experimental realization of quantum illumination. *Physical Review Letters*, 110 (15):153603, 2013. doi: 10.1103/PhysRevLett.110.153603.

[13] Florian Bischeltsrieder, Michael Würth, Johannes Russer, Markus Peichl, and Wolfgang Utschick. Engineering constraints and application regimes of quantum radar. *IEEE Transactions on Radar Systems*, 2:197–214, 2024. doi: 10.1109/TRS.2024.3361048.

[14] David Luong, Sreeraman Rajan, and Bhashyam Balaji. Entanglement-based quantum radar: From myth to reality. *IEEE Aerospace and Electronic Systems Magazine*, 35(4): 22–35, 2020. doi: 10.1109/MAES.2020.2970261.

[15] Saikat Guha and Baris I. Erkmen. Gaussian-state quantum illumination receivers. *Physical Review A*, 80:052310, 2009. doi: 10.1103/PhysRevA.80.052310.

[16] David Luong, Bhashyam Balaji, and Sreeraman Rajan. Biomedical sensing using quantum radars based on Josephson parametric amplifiers. In *Proceedings of the 2021 International Applied Computational Electromagnetics Society Symposium (ACES)*, pages 1–4, Hamilton, ON, Canada, 2021.

[17] David Luong, Ian W. K. Lam, Bhashyam Balaji, and Sreeraman Rajan. Quantum interferometric radar for biomedical applications. In *Radar Sensor Technology XXVIII*. SPIE, 2024.

[18] Abdulmohsen Alsaui, Octavia A. Dobre, Neel Kanth Kundu, Abdulkarim Hariri, and Hyundong Shin. Quantum radar for ISAC: Sum-rate optimization. 2025.

[19] Mark A. Richards, James A. Scheer, and William A. Holm, editors. *Principles of Modern Radar, Vol. I: Basic Principles*. SciTech Publishing, Raleigh, NC, USA, 2010.

[20] Renzhi Yuan. A brief introduction to POVM measurement in quantum communications. arXiv preprint arXiv:2201.07968, 2022.

[21] David Luong and Bhashyam Balaji. Quantum two-mode squeezing radar and noise radar: Covariance matrices for signal processing. *IET Radar, Sonar & Navigation*, 14 (1):97–104, 2020. doi: 10.1049/iet-rsn.2019.0090.

[22] Christian Weedbrook, Stefano Pirandola, Raúl García-Patrón, Nicolas J. Cerf, Timothy C. Ralph, Jeffrey H. Shapiro, and Seth Lloyd. Gaussian quantum information. *Reviews of Modern Physics*, 84:621, 2012. doi: 10.1103/RevModPhys.84.621.

[23] D. N. Makarov. Theory for the beam splitter in quantum optics: Quantum entanglement of photons and their statistics, HOM effect. *Mathematics*, 10(24):4794, 2022. doi: 10.3390/math10244794.

[24] K. M. R. Audenaert, J. Calsamiglia, R. Muñoz-Tapia, E. Bagan, Ll. Masanes, A. Acín, and F. Verstraete. Discriminating states: The quantum Chernoff bound. *Physical Review Letters*, 98(16):160501, 2007. doi: 10.1103/PhysRevLett.98.160501.

[25] Carl W. Helstrom. Quantum detection and estimation theory. *Journal of Statistical Physics*, 1(2):231–252, 1969.

[26] Daniel Manzano. A short introduction to the Lindblad master equation. *AIP Advances*, 10(2):025106, 2020. doi: 10.1063/1.5115323.